

RESEARCH ARTICLE

Chromatin remodelers couple inchworm motion with twist-defect formation to slide nucleosomal DNA

Giovanni B. Brandani, Shoji Takada *

Department of Biophysics, Graduate School of Science, Kyoto University, Kyoto, Japan

* takada@biophys.kyoto-u.ac.jp



Abstract

ATP-dependent chromatin remodelers are molecular machines that control genome organization by repositioning, ejecting, or editing nucleosomes, activities that confer them essential regulatory roles on gene expression and DNA replication. Here, we investigate the molecular mechanism of active nucleosome sliding by means of molecular dynamics simulations of the Snf2 remodeler translocase in complex with a nucleosome. During its inchworm motion driven by ATP consumption, the translocase overwrites the original nucleosome energy landscape via steric and electrostatic interactions to induce sliding of nucleosomal DNA unidirectionally. The sliding is initiated at the remodeler binding location via the generation of a pair of twist defects, which then spontaneously propagate to complete sliding throughout the entire nucleosome. We also reveal how remodeler mutations and DNA sequence control active nucleosome repositioning, explaining several past experimental observations. These results offer a detailed mechanistic picture of remodeling important for the complete understanding of these key biological processes.

OPEN ACCESS

Citation: Brandani GB, Takada S (2018) Chromatin remodelers couple inchworm motion with twist-defect formation to slide nucleosomal DNA. *PLoS Comput Biol* 14(11): e1006512. <https://doi.org/10.1371/journal.pcbi.1006512>

Editor: Alexey Onufriev, Virginia Tech, UNITED STATES

Received: May 18, 2018

Accepted: September 13, 2018

Published: November 5, 2018

Copyright: © 2018 Brandani, Takada. This is an open access article distributed under the terms of the [Creative Commons Attribution License](https://creativecommons.org/licenses/by/4.0/), which permits unrestricted use, distribution, and reproduction in any medium, provided the original author and source are credited.

Data Availability Statement: All relevant data are within the paper and its Supporting Information files.

Funding: This work was supported by JSPS KAKENHI grants [25251019 to ST, 16KT0054 to ST, and 16H01303 to ST] (<http://www.jsps.go.jp/english/>), by the MEXT as “Priority Issue on Post-K computer” to ST (<http://www.mext.go.jp/en/>), and by the RIKEN Pioneering Project “Dynamical Structural Biology” to ST (<http://www.riken.jp/en/>). The funders had no role in study design, data

Author summary

Nucleosomes are the protein-DNA complexes underlying Eukaryotic genome organization, and serve as regulators of gene expression by occluding DNA to other proteins. This regulation requires the precise positioning of nucleosomes along DNA. Chromatin remodelers are the molecular machines that consume ATP to slide nucleosome at their correct locations, but the mechanisms of remodeling are still unclear. Based on the static structural information of a remodeler bound on nucleosome, we performed molecular dynamics computer simulations revealing the details of how remodelers slide nucleosomal DNA: the inchworm-like motion of remodelers create small DNA deformations called twist defects, which then spontaneously propagate throughout the nucleosome to induce sliding. These simulations explain several past experimental findings and are important for our understanding of genome organization.

collection and analysis, decision to publish, or preparation of the manuscript.

Competing interests: The authors have declared that no competing interests exist.

Introduction

Eukaryotic genomes are compacted into the cell nucleus via the formation of nucleosomes, each of them consisting of ~147 base pairs (bp) of DNA wrapping around a protein histone octamer [1]. After having been initially considered as passive building blocks of chromatin organization, nucleosomes became to be recognized as active regulators of DNA transcription and replication [2]. An origin of this regulation is the steric effect that inhibits other DNA-binding proteins, such as transcription factors, from accessing nucleosomal DNA [3], suggesting the requirement of fine control of nucleosome positioning along the genomic sequence [2,4]. For instance, repositioning of nucleosomes enables the dynamic regulation of gene expression during cell differentiation [5] and in response to stresses such as heat shock [6,7]. While *in vitro* the nucleosome locations are solely determined by DNA mechanics [8,9], precise positioning *in vivo* is largely controlled by chromatin remodelers [2,4], which are ATP-dependent molecular machines [10,11]. High-resolution structures of some of these remodelers bound to nucleosomes were obtained very recently by cryo-EM [12–15]. While these static structures provide crucial insights, currently missing are the dynamic aspects of how these molecular machines work, on which the current study focus by molecular dynamics simulations.

Remodelers are molecular motors that consume ATP to perform a wide variety of functions related to genome organization [10,11]: facilitating nucleosome assembly [16] and precise spacing [17–19], controlling DNA accessibility via nucleosome sliding [20] or histone ejection [21], and nucleosome editing via exchange between different histone variants [22]. These activities enable remodelers to maintain chromatin organization after disruptive events such as replication [2,23], and to regulate gene expression via the dynamic control of nucleosome positions [6,7,21,24,25].

Although the changes in chromatin organization induced by remodelers have been widely documented [17,18], the precise molecular mechanisms are still far from being clear [10,11,26]. The complexity comes in part from the existence of a wide variety of remodelers with different structures and functions [11], which has led to several possible classifications into remodeler sub-families [27]. Each remodeler consists of many distinct domains, which act in concert to confer specificity to the remodeling activity (e.g. nucleosome sliding vs ejection) [10] and to fine-tune it via substrate recognition (e.g. of histone tail modifications) [28,29]. Despite this complexity, all remodelers share a conserved translocase domain [10]: an ATPase motor capable of unidirectional sliding along DNA via binding and hydrolysis of ATP between its two RecA-like lobes, structurally similar to those found in helicases [12,27]. The translocase domain of most remodelers binds nucleosomes at the superhelical location (SHL) 2 [12,13,30], i.e. two DNA turns away from the dyad symmetry axis (SHL 0) [31] (Fig 1A). Many remodelers induce sliding of nucleosomal DNA towards the dyad from the translocase binding location [30,32–34]. Sliding may represent a shared fundamental mechanism at the basis of most remodeling activities; the interactions with the additional domains would then confer specificity to the remodeler, allowing for substrate recognition and determining whether the final outcome is nucleosome repositioning, histone ejection or histone exchange [10,35]. For instance, recent experiments suggested that the INO80 remodeler causes histone exchange by sliding nucleosomal DNA from its translocase binding site around SHL 6 [14,15,34]. Therefore, the detailed characterization of active nucleosome sliding by the translocase domain would represent a significant step forward in our understanding of chromatin remodeling.

There is much experimental evidence suggesting that the translocase domain of remodelers, as well as some helicases, slides unidirectionally along DNA via an inchworm mechanism [10,36], which may also be viewed as a molecular ratchet [13,37], processing by 1 bp every

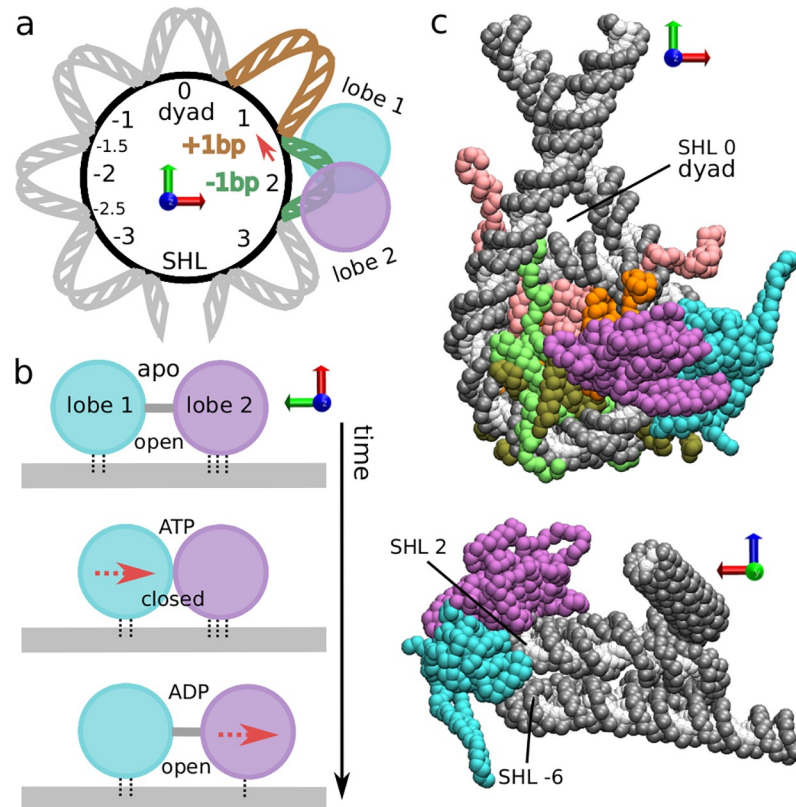


Fig 1. Structure of the translocase-nucleosome complex. (a) Cartoon where nucleosome regions are indicated by the number of DNA turns from the dyad symmetry axis; superhelical location (SHL) 0 corresponds to the dyad, the ATPase domain (lobe 1 in cyan, lobe 2 in purple) binds DNA at SHL 2, the strong histone-DNA contact points are located at the half-integer SHLs where the DNA minor groove faces the octamer, e.g. -1.5 and -2.5. For clarity, we only depict the region from SHL -4 to +4. To analyze DNA sliding, we track the base pair indexes Δbp_i at these contact points relative to the initial conformation. If, for example, nucleosome sliding starts with the motion of DNA at contact point 1.5 by 1 bp towards the dyad (red arrow), the contact index $\Delta bp_{1.5}$ will increase from ~ 0 to ~ 1 , and this will also indicate the formation of a +1bp defect at SHL 1 (in brown) and a -1bp twist defect at SHL 2 (in green), respectively accommodating an extra and a missing base pair relative to the reference nucleosome conformation in the crystal structure with PDB id 1KX5. (b) Inchworm mechanism of translocase motion along DNA. ATP binding induces a conformational change from open to closed, with the motion of lobe 1 towards lobe 2 by 1 bp, due to the weaker DNA contacts of the former. ATP hydrolysis weakens the lobe 2-DNA contacts and induces opening via the motion of lobe 2 away from lobe 1 by 1 bp. ADP release completes the cycle. (c) Two views of the initial Snf2-nucleosome structure for our coarse-grained MD simulations: DNA backbone (phosphate and sugar groups) in gray, bases in white, translocase lobes in cyan and purple, histones H3 in pink, H4 in orange, H2A and H2B in light and dark green respectively (in top snapshot only). From the bottom view it is possible to appreciate the contacts between the translocase lobe 1 and the opposite DNA gyre at SHL -6. All nucleosome orientations are indicated by the red, green and blue axes.

<https://doi.org/10.1371/journal.pcbi.1006512.g001>

ATP cycle. A minimal inchworm model requires 3 distinct chemical states, apo, ATP-bound, and ADP-bound, which are coupled to conformational changes of the translocase (Fig 1B). The two lobes are either distant in the open form or in contact in the closed form. On top, conformational changes modulate interaction strengths with DNA [37]. To translocate along DNA in the direction from lobe 1 to lobe 2 (which would correspond to sliding nucleosomal DNA in the direction from SHL 2 towards the dyad, as in most remodelers [12]), ATP binding to the translocase first induces the transition from an open to a closed conformation (first and second cartoons in Fig 1B). During closure, lobe 2-DNA interactions are stronger than those of lobe 1, so that lobe 1 will detach from the DNA and move towards lobe 2 by 1 bp, which maintains its position. Then, ATP hydrolysis is accompanied by weakening of the lobe 2

interactions with DNA relative to those of lobe 1, so that during the conformational change from the closed to the open state lobe 2 now moves away from lobe 1 by 1 bp (third cartoon in Fig 1B). The cycle is then completed by the release of ADP and the change of the interaction strengths to their initial apo-state values. This mechanism was firstly suggested for helicases from their crystal structures, which show ATPase closure and changes in lobes-DNA interactions as a function of the chemical state [36,37]. For remodelers, the same mechanism was suggested based on the structural similarity to helicases [11,12,27] and the recent cryo-EM structures of nucleosome-bound remodelers in the open and closed conformations [12,13]. However, while the inchworm model can explain the motion of remodelers along naked DNA [38], its application to nucleosome repositioning is far from trivial, since such motion would eventually result into steric clashes between the remodeler and the histone octamer. Furthermore, complete nucleosome repositioning necessarily involves breakage of the many histone-DNA contacts that stabilize the nucleosome structure [31], and it is not clear how the remodeler may perturb the contacts far away from the binding location at SHL 2.

Experimental studies have also highlighted many diverse structural changes of the nucleosome occurring during remodeling, such as DNA twisting [26], loops [39] or histone deformations [40], suggesting these may be directly responsible for nucleosome sliding. Interestingly, similar structural changes are also believed to mediate spontaneous sliding [41]. Therefore, insights from research on spontaneous nucleosome repositioning may shed light into the more complex active case. Indeed, DNA sliding on nucleosomes can also be simply driven by thermal fluctuations [42]. Modes of nucleosome repositioning can be classified in two types depending on whether sliding is accompanied by the rotation of DNA around its axis [43]. In the rotation-uncoupled mode, sliding proceeds via large steps of about a DNA turn (~10 bp) [43–45], possibly facilitated by the formation of loops [44,45]. On the other hand, in the rotation-coupled mode, DNA sliding proceeds at small steps of 1 bp via a screw-like motion [43], facilitated by the formation of twist defects [1,46–50]. Twist defects are the structural deformations of DNA allowing to accommodate different numbers of base pairs between the strong histone-DNA contact points, which correspond to half-integer SHL locations [31,48]. Between two adjacent contact points, while canonical DNA turns contains ~10-bp, 9 bp (a missing bp) or 11 bp (an extra bp) may also be accommodated; we refer to these deformations as -1bp and +1bp twist defects respectively (see an example illustrated in Fig 1A, where the anti-clockwise motion of DNA at the contact point at SHL 1.5 generates a -1bp defect at SHL 2, in green, and a +1bp defect at SHL 1, in brown). The spontaneous formation and propagation of twist defects around the nucleosome causes repositioning by 1 bp at the time [47,49]. Notably, the small characteristic step sizes observed during nucleosome sliding by the ISWI and RSC remodelers [20,51] argues in favor of a role for DNA twisting in the molecular mechanism [26]. Furthermore, having the same step size, active sliding via twist defects is compatible with the inchworm motion of the translocase domain. While some remodelers have been shown to induce the formation of large DNA loops in nucleosomes [39], this may be due to interactions with extra domains in the remodeler, and their presence should not rule out the contribution of twist defects to chromatin remodeling.

Due to the ubiquitous importance of remodelers for chromatin organization, gene expression and replication [2], the detailed understanding of their molecular mechanism of action would be extremely valuable. Coarse-grained molecular dynamics (MD) simulations [52] represent an ideal tool for approaching this problem, since their resolution can be high enough to accurately represent the potential key steps occurring during active nucleosome repositioning [43,49,53], while achieving a speed-up of several orders of magnitude relative to all-atom simulations [52], for which the system size and the relevant time scales would result in an exceedingly large computational cost. Notably, coarse-graining approaches have been successfully

applied to the study of nucleosome dynamics [9,54–56], including spontaneous repositioning [43,45,49], and ATP-dependent molecular motors [53,57].

In this work, we investigate the fundamental mechanism of active repositioning in a minimal system consisting of the ATPase-translocase domain of the Snf2 remodeler from yeast in complex with the nucleosome [12]. Firstly, we test that our model can reproduce the expected inchworm mechanism and unidirectional sliding during ATP consumption. By comparing to the spontaneous case, we show how the remodeler induces directed repositioning by modifying the nucleosome free energy landscape via steric effects and long-range electrostatic interactions, explaining past experimental data on Snf2 mutants [12]. Nucleosome repositioning occurs by coupling the ATPase inchworm motion to the formation and propagation of twist defects starting from the remodeler binding location at SHL 2. Finally, we reveal how DNA sequence can be exploited to control the kinetics of the system, consistently with its role in determining the repositioning outcome of many remodelers [18,58,59].

Results

MD simulations of remodeler translocase sliding on naked and nucleosomal DNA via an inchworm mechanism

We performed coarse-grained MD simulations of the ATP-dependent translocase domain of the Snf2 remodeler both on naked DNA and when bound to nucleosomes (Fig 1C). The nucleosome model is the same as that previously employed to study spontaneous nucleosome repositioning [43,49], whereas the remodeler model and its interactions with the DNA are based on the cryo-EM structure of the Snf2-nucleosome complex with PDB id 5X0Y [12]. Our computational model coarse-grains proteins at the level of individual residues [60] and DNA at the level of sugar, phosphate, and base groups, capturing the sequence-dependent flexibilities of base steps [61,62] (see the [Materials and Methods](#) section and Refs. [43,60,61] for more details). In the first set of simulations, the nucleosomal DNA consists of a 2-bp periodic sequence formed by repeating ApG base steps, polyApG. This sequence was chosen because it was shown to display an intermediate flexibility on the nucleosome [49], and it is used as a reference against which we compare other more experimentally and biologically relevant sequences. In particular we consider the effects due to strong positioning along DNA (601 sequence [63]), and the introduction of poly(dA:dT) tracts and TpA repeats.

Based on the inchworm model (Fig 1B), each remodeler chemical state (apo, ATP or ADP) corresponds to slightly different force-field parameters of the coarse-grained potential, and we simulate an ATP cycle (apo→ATP→ADP→apo) via switching the potential during the MD simulation, a common strategy in coarse-grained studies of molecular motors [57,64]. Initially, in the open apo state, the remodeler configuration and the strengths of the interactions between ATPase lobes and DNA are as found in the cryo-EM structure with PDB id 5X0Y [12]; then, switching to the ATP-bound potential enhances the attraction between the two lobes, favoring the closed conformation of the remodeler. ATP hydrolysis is emulated by switching to the ADP-bound potential, which reduces the lobe 2-DNA interactions by a factor of 0.8 and weakens the attractive interaction between the two lobes to favor the open conformation. In all our MD trajectories (40 on naked DNA, 100 on nucleosome for each DNA sequence), switching from apo to ATP states occurs at time 0 after 2×10^7 MD equilibration steps in the open conformation, ATP hydrolysis occurs after 10^7 MD steps, which are sufficient for the full relaxation of the system in the closed conformation, and finally switching back to the apo state occurs after 10^7 steps (which are sufficient to observe translocase opening). This simulation protocol is mainly motivated by the mechanism of helicase sliding identified from the analysis of crystal structures [37]. More details are provided in the [Materials and Methods](#) section.

To analyze the repositioning dynamics in our MD trajectories, we track the motion of the DNA base pairs relative to the two individual ATPase lobes and relative to the histone octamer at the 14 histone-DNA contact points, located at the half-integer SHLs where the DNA minor groove faces the octamer. We refer to these collective variables as the contact indexes: Δbp_{L1} and Δbp_{L2} for the remodeler lobes and Δbp_i for the histone contacts, where i is the half-integer valued SHL of the contact (these contacts will be indicated by their SHL value, e.g. contact point 1.5). As in our previous work [49], the nucleosome contact indexes are evaluated relative to the 147-bp conformation found in the crystal structure with PDB id 1KX5 [65], which does not display twist defects. The contact indexes take fractional values because they are continuous collective variables computed from the system coordinates [49] (see Supporting Information S1 Text for the full description of their calculation). Using these variables, we can fully characterize the remodeler's inchworm dynamics, the sliding of DNA in the nucleosome, and the potential role played by twist defects. These DNA deformations are distributed around integer-valued SHLs lacking direct histone-DNA contacts, and can accommodate either an extra base pair relative to the 1KX5 reference (+1bp defect), or a missing base pair (-1bp defect) [1,46,47,66]. A twist defect at SHL i can be simply evaluated by the difference between the neighboring contact indexes ($i-1/2$ and $i+1/2$): a defect value close to zero corresponds to the standard non-defect case, a value close to 1 to an extra base pair and a value close to -1 to a missing base pair (see an example in Fig 1A).

In this section, we present the simulation results of both Snf2-naked DNA and Snf2-nucleosome systems, but focusing on the motion of the remodeler relative to the DNA. In Fig 2A, we show that by switching between the remodeler chemical states during the MD simulation, this can slide along both naked and nucleosomal DNA by 1-bp (as evidenced by the change in the average lobe contact index during the ATP cycle). While sliding on naked DNA is not a key function of remodelers, this process has been documented in experiments [38]. Interestingly, we note that under the current computational settings sliding by 1 bp by the end of an ATP cycle occurs with higher probability when in complex with nucleosomes (98%) than when on naked DNA (45%), whereas in the remaining cases the remodeler simply goes back to its original position.

Fig 2B displays two representative trajectories (one on the naked DNA and one on the nucleosome) projected onto the contact indexes of the two separate ATPase lobes. In both cases, this projection clearly highlights the inchworm motions. Specifically, starting from the apo state in the open conformation (bottom left in the figure), switching the potential to the ATP state induces the closure of the remodeler, with lobe 1 moving by 1 bp towards lobe 2, which maintains its position due to its stronger grip to the DNA (bottom right). Then, simulating ATP hydrolysis via switching to the ADP-state potential induces the domain opening, but since the lobe 2-DNA interactions are also decreased, now it is this lobe that usually moves by 1 bp away from lobe 1 (top right). Switching again to the apo-state potential simply restores the original lobes-DNA interaction strengths, maintaining the same open configuration and completing a full ATP cycle with the remodeler shifted by 1 bp relative to where it started. On naked DNA, this mechanism is sufficient to explain the translocase's unidirectional motion (see S1 Movie for a visualization of the trajectory in Fig 2B). However, what is not clear from this analysis is how the translocase motion may induce sliding of nucleosomal DNA; the next sections are devoted to the characterization of the complete active repositioning process.

Remodelers couple inchworm motion to nucleosome sliding via steric and electrostatic interactions

Our MD simulations show that the ATP-driven translocase closure is followed by sliding of nucleosomal DNA. Specifically, the DNA at the remodeler binding location slides

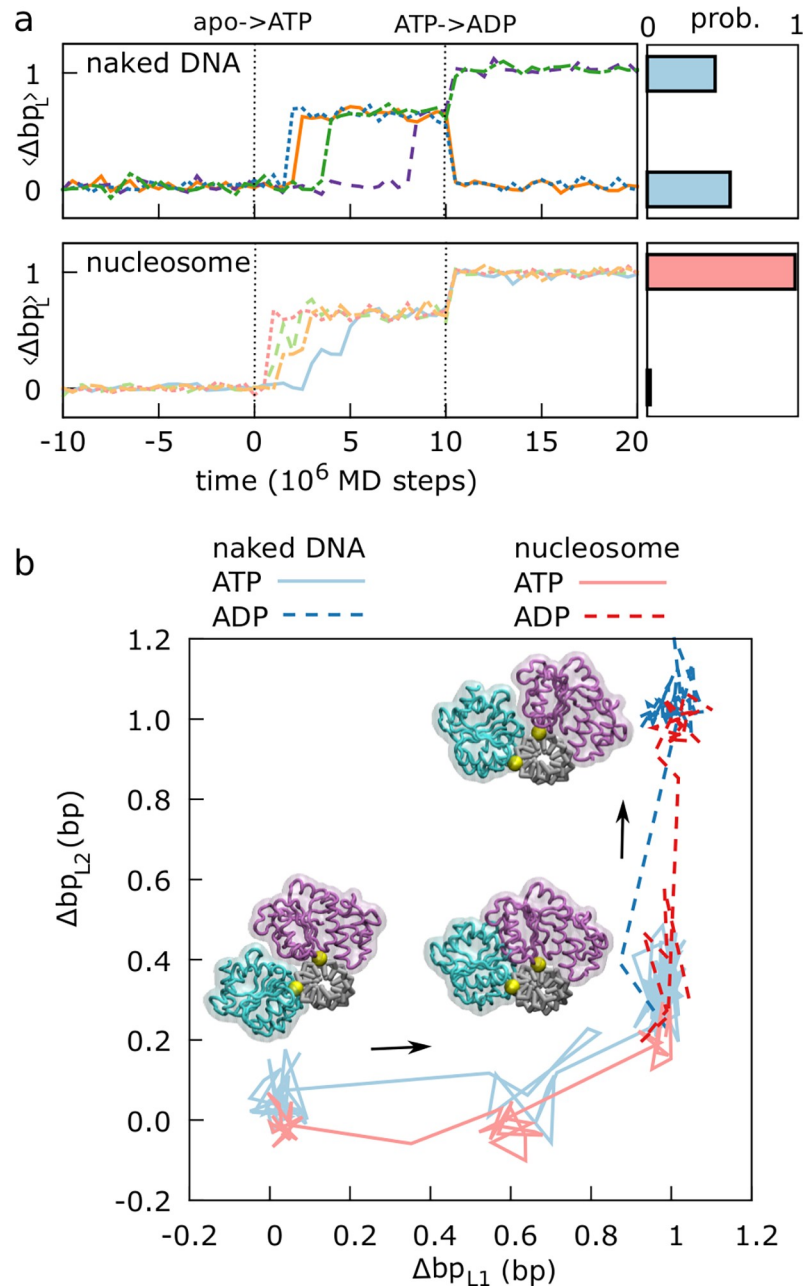


Fig 2. Snf2 translocase motion relative to DNA via an inchworm mechanism. (a) Representative trajectories (indicated by different colors) of the average lobe contact index $\langle \Delta bp_L \rangle = (\Delta bp_{L1} + \Delta bp_{L2})/2$ during the ATP cycle in our MD simulations (ATP binding occurs after equilibration at time 0, hydrolysis occurs after 10^7 MD steps) on naked (upper left) and nucleosomal (lower left) DNAs with polyApG sequence. In both cases we find unidirectional motions; a 1 bp step of the translocase in direction from lobe 1 to lobe 2 occurs every ATP cycle with probabilities of ~ 0.45 and ~ 0.98 on naked DNA (upper right) and on nucleosomal DNA (lower right), respectively. Probabilities are calculated from the histograms of the integer values closest to $\langle \Delta bp_L \rangle$ at 2×10^7 MD steps after ATP binding, out of 40 and 100 MD simulations on naked DNA and nucleosome respectively. (b) Projections of two representative trajectories (blue for naked, red for nucleosomal DNAs) on the lobe contact indexes Δbp_{L1} and Δbp_{L2} (lighter solid lines for the ATP state, darker dashed lines for the ADP state after hydrolysis), highlighting the inchworm mechanism. Snapshots of translocase moving on naked DNA are also shown (lobe 1 in cyan, lobe 2 in purple, DNA in gray, two reference phosphates in yellow).

<https://doi.org/10.1371/journal.pcbi.1006512.g002>

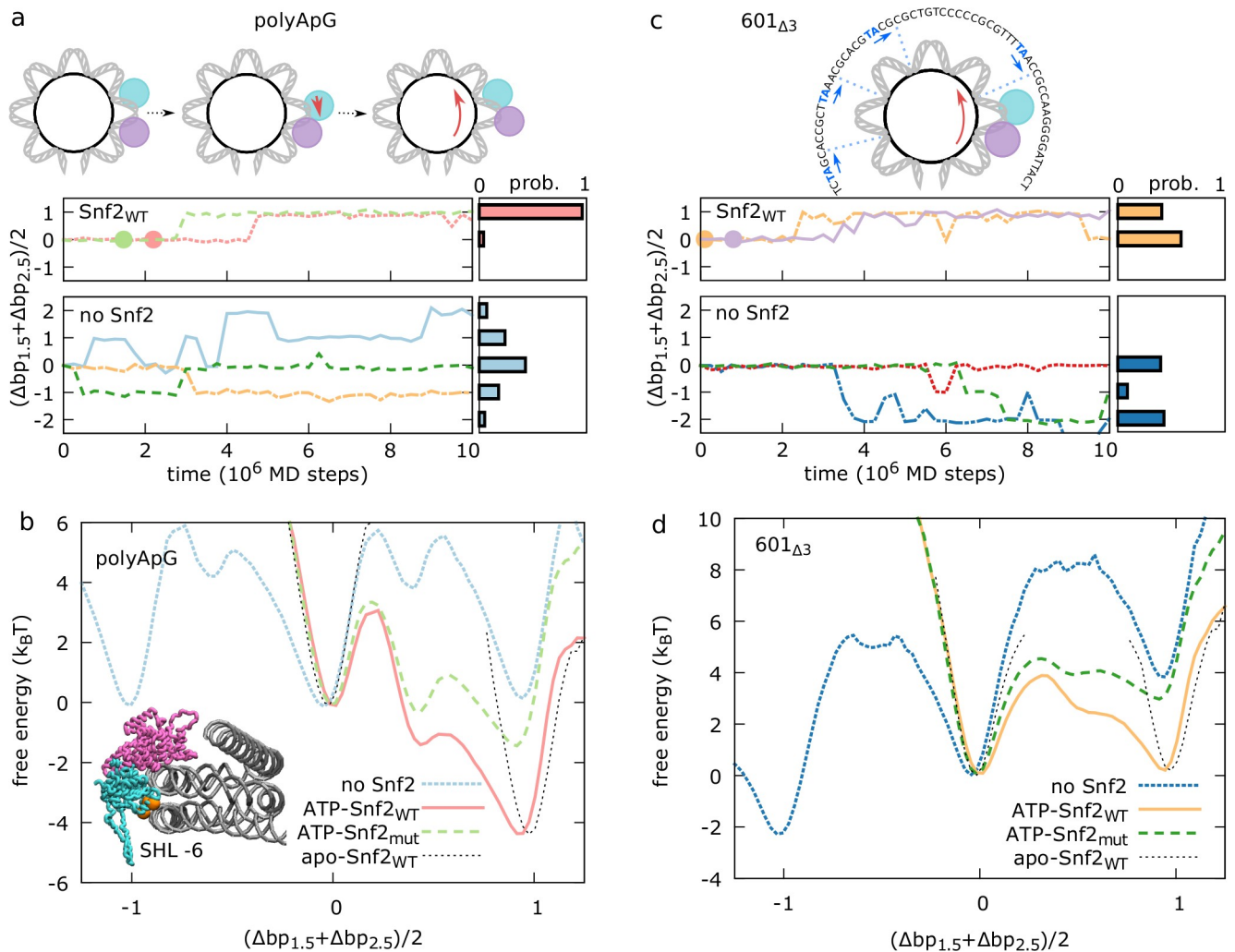


Fig 3. Mechanism of directed nucleosomal DNA sliding by Snf2. (a,c) For polyApG (a) and 601 Δ_3 (c) sequences, we show representative trajectories (indicated by different colors) of the average contact index at SHL 2, $(\Delta bp_{1.5} + \Delta bp_{2.5})/2$, as a function of time (left panel) and the probabilities of $(\Delta bp_{1.5} + \Delta bp_{2.5})/2$ at 10^7 MD steps after ATP binding computed from 100 trajectories (right), for the remodeler-bound case (upper), and in the absence of remodeler (spontaneous sliding) (lower). For the remodeler case, we report only the portion of trajectory in the ATP state, where nucleosome sliding occurs after the translocase closure (indicated by the circles). (b,d) For polyApG (b) and 601 Δ_3 (d) sequences we report the free energy profiles along the average contact index at SHL 2 for different systems: spontaneous sliding in the absence of the remodeler (no Snf2), in the complexes with the bound open apo-state Snf2 (apo-Snf2_{WT}), the closed ATP-bound Snf2 (ATP-Snf2_{WT}), and the closed ATP-bound K855E-R880E-K885E charge mutant Snf2 (ATP-Snf2_{mut}). Errors on the free-energy profiles are on the order of ~ 0.3 k_BT. The cartoons in panel a indicate how the inchworm motion of the translocase (lobe 1 in cyan, lobe 2 in purple) is coupled to nucleosome sliding. The structure of the Snf2-nucleosome complex in the inset in panel b highlights the location of the K855, R880 and K885 residues (orange) targeted by the mutation. In panel c we also displayed the central 63 base pairs of the 601 Δ_3 sequence highlighting the location of the T_pA positioning steps within the Snf2-nucleosome complex (in blue). In the initial configuration for the 601 Δ_3 simulations, the DNA is shifted by 3 bp relative to the optimal structure with PDB id 5X0Y (with the T_pA steps located where the DNA minor groove faces the histone octamer, indicated with a blue dashed line).

<https://doi.org/10.1371/journal.pcbi.1006512.g003>

unidirectionally towards the dyad, as indicated by the 1-bp increase in the average nucleosome contact index around SHL 2, $(\Delta bp_{1.5} + \Delta bp_{2.5})/2$ (see two representative trajectories and the cumulative distribution at the end of the ATP-state in Fig 3A, upper panel). This is consistent with the directionality of repositioning observed in experimental studies [32] and with what expected from the comparison with the structure of helicases [12]. On the other hand, in the absence Snf2, sliding of the same polyApG nucleosomal DNA occurs in a random direction (Fig 3A, lower panel).

To better characterize the origin of the unidirectional motion, in Fig 3B, we compare the free-energy profiles of nucleosome sliding along the average contact index around SHL 2 for different scenarios. In the absence of Snf2, as expected for the uniform polyApG sequence and the random motion reported in Fig 3A, sliding by 1 base pair in either direction does not change the free energy of the system, but it involves climbing significant free-energy barriers ($\sim 6 k_B T$). The presence of the remodeler modifies the original nucleosome landscape in a chemical-state-dependent fashion. In the initial open conformation before ATP binding, there is a single free-energy minimum at $(\Delta bp_{1.5} + \Delta bp_{2.5})/2 = 0$, so that nucleosomal DNA sliding is strongly inhibited. Instead, after ATP binding and translocase closure, a second deeper free-energy minimum appears around $(\Delta bp_{1.5} + \Delta bp_{2.5})/2 = 1$, favoring DNA sliding towards the dyad. After the last opening conformational change following ATP hydrolysis, the nucleosome landscape returns to have a single free-energy minimum now at $(\Delta bp_{1.5} + \Delta bp_{2.5})/2 = 1$, so that further sliding is inhibited. The switching among these different free-energy landscapes reveals a clear ratchet mechanism, as often employed for the theoretical modeling of molecular motors [67]. The changes in the free energy profiles can be in part explained by the inchworm motion of the translocase domain and steric effects. In the open conformation, DNA sliding at SHL 2 by 1 bp in either direction would cause steric overlap between lobe 2 and histone octamer on one side or overlap between lobe 1 and the opposite DNA gyre around SHL -6 on the other side (see inset in Fig 3B), blocking nucleosome repositioning and explaining the single free energy minimum when Snf2 is in the apo state. Since the translocase closure upon ATP binding involves the motion of lobe 1 towards lobe 2, DNA sliding is now allowed to occur towards the dyad, causing the translocase to swing on the opposite side of its binding location (see cartoons in Fig 3A). However, this argument does not explain the large extent to which the closed ATPase favors unidirectional repositioning, i.e. the decrease in free energy by $\sim 4 k_B T$ from $(\Delta bp_{1.5} + \Delta bp_{2.5})/2 = 0$ to 1.

From the crystal structure of the nucleosome-bound Snf2 remodeler [12], it was shown that apart from the main interactions at SHL 2, the translocase domain also interacts with the opposite DNA gyre around SHL -6 via long-range electrostatics mediated by residues K855, R880 and K885, located within lobe 1 (see bottom view in Fig 1C and inset in Fig 3B). It was also experimentally shown that changing these residues from positively- to negatively-charged markedly reduced the remodeling activity of Snf2 [12]. To investigate this effect, we performed MD simulations where the three key residues have all been mutated to glutamic acid (K855E-R880E-K885E mutant). While still possible, DNA sliding around SHL 2 is no longer accompanied by a large decrease in free energy (Fig 3B). This change can be understood in terms of the movement of the ATPase lobe 1 during repositioning. In the open state, lobe 1 is close to the contact point 1.5 and also interacts with the opposite gyre at SHL -6 via the basic patch in wild-type (WT) Snf2 (K855, R880 and K885). After ATP binding, lobe 1 moves by 1 bp towards lobe 2, becoming further apart from both contact point 1.5 and the DNA at SHL -6, weakening the electrostatic interaction (specifically, the average distance between the center of mass of the lobe 1 patch and the DNA phosphate backbone increases from $\sim 6.1 \text{ \AA}$ to $\sim 8.3 \text{ \AA}$ upon translocase closure). The sliding of nucleosomal DNA causes lobe 1 to swing back towards the dyad, restoring also the original interactions between the basic patch and SHL -6. Comparing to the initial open apo structure, the translocase closure and subsequent sliding of DNA at SHL 2 makes it appear that lobe 2 moved by 1 bp towards lobe 1, and not the opposite. Notably, this observation is consistent with the recent cryo-EM structure of the nucleosome-Chd1 complex in the presence of an ATP analog [13], where lobe 1 overlaps with the corresponding lobe in the open conformation of the Snf2 remodeler [12], whereas lobe 2 appears to have moved by 1 bp [13].

While so far we only considered a simple uniform polyApG sequence, genomes are rich in positioning motifs that contribute to specify the optimal location of nucleosomes along DNA [4]. These motifs, such as T/A base steps periodically spaced every 10 bp, cause the intrinsic bending of DNA, which lowers the free energy cost of nucleosome assembly, and favor a specific rotational setting, as they preferentially locate where the DNA minor groove faces the histone octamer [9]. These signals strongly inhibit nucleosome sliding relative to random DNA sequences, since repositioning would proceed either by DNA screw-like motion via a high-energy intermediate with a non-optimal rotational setting [47,49], or via alternative repositioning mechanisms uncoupled with DNA rotations, which involve the energetically-costly breakage of many histone-DNA contacts [43,45]. Nevertheless, chromatin remodelers are still able to actively reposition nucleosomes made with strong positioning sequences such as 601 [12,20,63].

To investigate the robustness of the active repositioning mechanism against changes in DNA sequence, we next run MD simulations of Snf2 in complex with nucleosomes made with the 601 sequence [63]. In the starting configuration, we shifted the DNA by 3 bp relative to the optimal configuration found in the 5X0Y structure, in the direction from the remodeler site towards the dyad. We refer to this sequence as 601_{Δ3}. Because of the non optimal location of the T/A steps relative to the histone octamer (see cartoon in Fig 3C), starting from here in the absence of the remodeler will be most likely followed by sliding backward away from the dyad, i.e. towards the optimal configuration (in about half of the cases within 10⁷ MD steps, Fig 3C, lower panel). Instead, not only the remodeler prevents backward sliding, but upon ATP binding, in about half of the cases, it can also induce sliding of nucleosomal DNA forward towards the dyad (Fig 3C, upper panel), in the same way as observed with the uniform polyApG sequence. A comparison of the free-energy landscapes along DNA sliding at SHL 2 with and without remodeler (Fig 3D) shows indeed that in the case without remodeler the free energy strongly increases with sliding forward towards the dyad and decreases away from the dyad, whereas the closed translocase is able to lower the free energy cost of forward sliding to ~0 k_BT, while preventing sliding backward in the opposite direction via steric effects. The free energy profile obtained with the K855E-R880E-K885E Snf2 bound to 601_{Δ3} nucleosomes, shows that this mutant cannot slide these strong positioning sequences, due to an extra free energy penalty of ~3 k_BT upon sliding by 1 bp. This is consistent with the results from experiments on similar Snf2 charge mutants sliding 601 nucleosomes [12]. While the limitations of our computational model (e.g. the assumptions on the precise ATP hydrolysis kinetics) prevent us from making quantitative predictions of remodeling activity, our simulations provide a mechanistic understanding of the important role of electrostatic interactions in directing repositioning [12].

To show that Snf2 is also able to reposition natural genomic sequences (both polyApG and 601 are artificial), we also performed MD simulations using the weakly positioning 5S rDNA sequence commonly studied experimentally [68], starting with a nucleosome at the expected equilibrium location [69]. Even in this case, remodeling by 1 bp at the end of an ATP cycle occurs successfully in most trajectories (15 out of 20).

Apart from the interactions between lobe 1 and DNA at SHL -6, the cryo-EM structure of Snf2 also highlighted electrostatic contacts between the H4 N-terminal tail and an acidic patch located on lobe 2 (E1069, D1121) [12]. Analyzing our trajectories, we found that indeed the tip of the H4 tail often localizes in the vicinity of the Snf2 acidic patch (~1 nm distance between C α atoms). However, these interactions do not have any particular correlation with the sliding of nucleosomal DNA or the inchworm motion of the remodeler, suggesting that they do not play a fundamental role. Although mutations in the H4 tail do have a minor effect on the remodeling activity of the Snf2 translocase [12], we suspect this should be mainly due to a reduction in the binding affinity to the nucleosome.

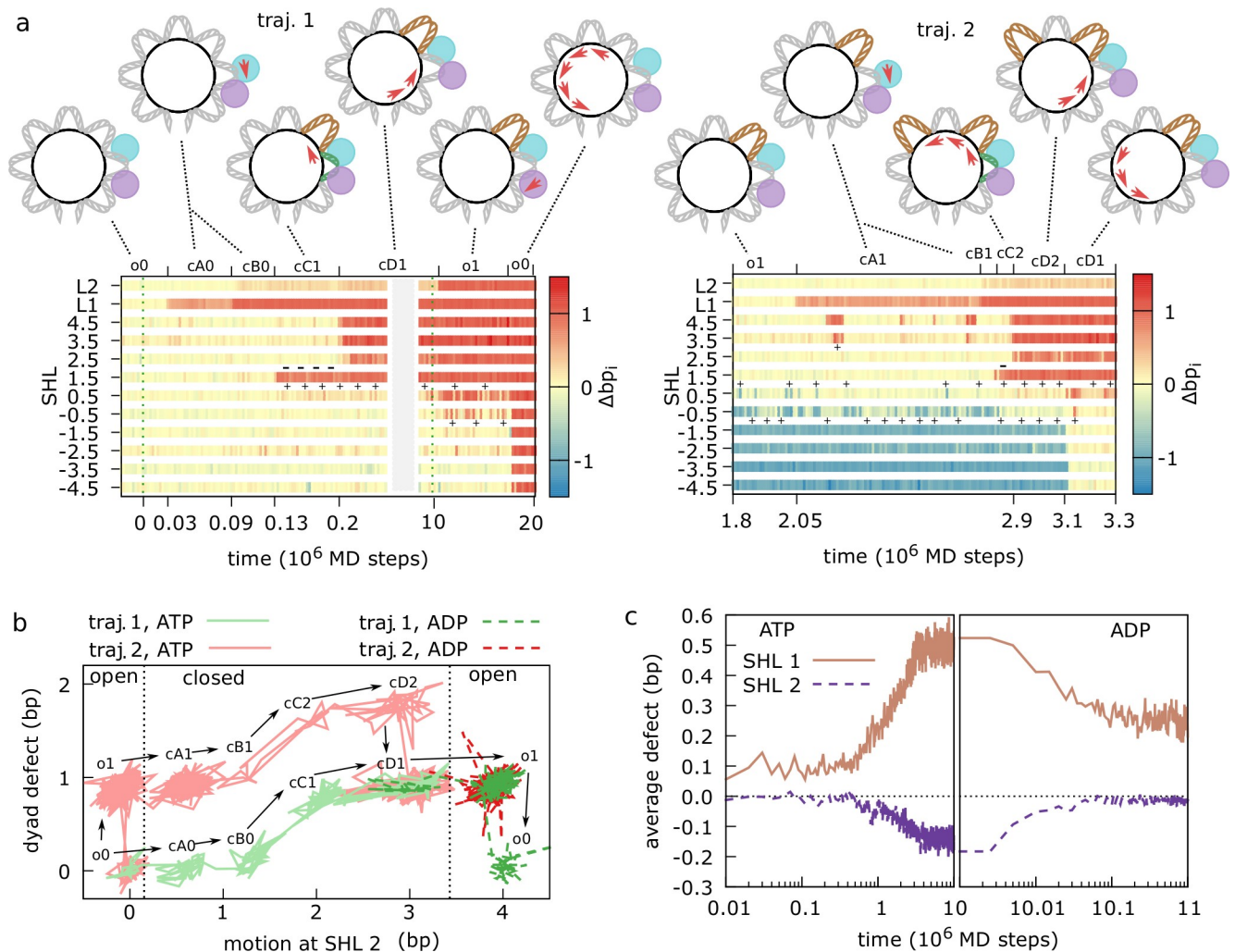


Fig 4. Active nucleosome repositioning via twist defect propagation for polyApG sequence. (a) Timelines of the translocase (L1 and L2) and nucleosome contact indexes (SHL -4.5 to 4.5) for two representative trajectories where nucleosomal DNA slides by 1 bp relative to the initial configuration. The intermediate configurations along the repositioning pathway are indicated by the corresponding labels (described in the main text) and cartoons. The key twist defects facilitating repositioning are highlighted by a plus sign for +1bp defects (in brown in the cartoons) and by a minus sign for -1bp defects (in green in the cartoons). DNA and translocase lobes (1 in cyan, 2 in purple) motions are indicated by red arrows. ATP binding occurs at time 0, whereas ATP hydrolysis occurs at 10^7 MD steps. (b) 2-dimensional projections of the trajectories in panel (a) (traj. 1 in green, traj. 2 in red; lighter solid lines for the ATP state, darker dashed lines after hydrolysis; time increases in the direction indicated by the arrows). The x-axis represents the sum of the translocase and nucleosome contact indexes around the remodeler binding location at SHL 2: $\Delta bp_{L1} + \Delta bp_{L2} + \Delta bp_{1.5} + \Delta bp_{2.5}$. The y-axis represents the size of the twist defects at the three central SHLs: $\Delta bp_{1.5} - \Delta bp_{-1.5}$. The key metastable states along the repositioning pathways, indicated by the same labels used in panel a, can be well distinguished as individual clusters on this low-dimensional projection. (c) Twist defect coordinates at SHL 1 ($= \Delta bp_{1.5} - \Delta bp_{0.5}$, brown, solid line) and SHL 2 ($= \Delta bp_{2.5} - \Delta bp_{1.5}$, purple, dashed) averaged over 100 MD trajectories as a function of time, showing how twist defects are formed after ATP binding and translocase closure (at 0 MD steps; panel c, left), and how they are released after hydrolysis and translocase opening (at 10^7 MD steps; panel c, right).

<https://doi.org/10.1371/journal.pcbi.1006512.g004>

Nucleosome repositioning proceeds via the formation and propagation of twist defects from the remodeler binding location

So far, we focused on the inchworm motion of the translocase domain and on nucleosomal DNA sliding at the SHL 2 binding site, establishing how these two are tightly coupled. However, a full characterization of the repositioning mechanism requires the analysis of DNA sliding at the individual histone-DNA contact points on the entire nucleosome. In Fig 4A, we plot the timelines of the contact index coordinates of both remodeler and nucleosome for two

representative trajectories during which repositioning by 1 bp occurs. These plots show how nucleosomal DNA sliding is initiated near the translocase binding location at the contact point at SHL 1.5, with the creation of opposite-type twist defects at the neighboring SHLs. The diffusion of these defects then completes repositioning of the entire nucleosome. To aid the understanding of the dynamics, we label the key metastable conformations of the system according to the following rules: the first letter, o or c, corresponds respectively to open or closed translocase conformation; when it is closed (c), the domain can adopt distinct configurations with DNA and histone octamer within its binding site at SHL 2, which will be indicated by a capital letter as A, B, C or D (see below for definition); finally, a last integer number, 0, 1 or 2, indicates the number of +1bp defects which may form near the dyad at the three central SHLs (SHL -1, 0, and +1, these defects are most favorably found at SHLs +/-1).

In the first trajectory (the left panel in Fig 4A), starting from an open translocase bound to a nucleosome in a standard 1KX5-like configuration lacking twist defects (state o0), switching to the ATP-bound potential at time 0 quickly induces the closure of the remodeler via the motion of lobe 1 towards lobe 2 (0.03×10^6 MD steps, state cA0). In this first closed configuration, the lobe 1-DNA interface is destabilized relative to the one observed in the reference 5X0Y structure and the motion towards lobe 2 is only partial ($\Delta b_{pL1} \sim 0.6$). Only after some time (0.09×10^6 MD steps) the motion of lobe 1 is complete ($\Delta b_{pL1} \sim 1$, state cB0). From this closed configuration, we observe motion of nucleosomal DNA towards the dyad relative to the histone octamer starting from SHL 1.5 (0.13×10^6 MD steps, state cC1), causing the accumulation of an extra base pair at SHL 1, and a missing base pair at SHL 2 (where the remodeler is bound). Soon afterwards (0.2×10^6 MD steps), the nucleosomal DNA further slides from the remodeler site up to the closest nucleosome entry/exit, releasing the -1bp defect (state cD1). As highlighted in the previous section, while these two steps do not involve remodeler's motion relative to the DNA, the DNA motion relative to the histone octamer causes the remodeler to swing by 1 bp towards the dyad and enables to re-establish the electrostatic contacts between lobe 1 and SHL -6, which were lost during the initial ATPase closure. State cD1, for the polyApG sequence considered here, is the most stable configuration among the closed ones. Repositioning is usually completed only after ATP hydrolysis (10×10^6 MD steps), which causes translocase opening via lobe 2 motion by 1 bp (state o1) (the full pathway is $o0 \rightarrow cA0 \rightarrow cB0 \rightarrow cC1 \rightarrow cD1 \rightarrow o1 \rightarrow o0$). The very last step consists of the sliding of nucleosomal DNA from the translocase up to the far nucleosome entry/exit, releasing the +1bp defect near the dyad (state o0, see S2 and S3 Movies for visualizations of this trajectory). The second trajectory (Fig 4A, right) is qualitatively similar to the first, except that all states have an additional defect near the dyad at the starting time (the full pathway is then $o1 \rightarrow cA1 \rightarrow cB1 \rightarrow cC2 \rightarrow cD2 \rightarrow cD1 \rightarrow o1$ for trajectory 2). In particular, motion at the remodeler and nucleosome contact points proceeds in the same order. These two pathways are representative of the most common ones found in our 100 MD trajectories: the first one being observed in 16 cases, while the second one in 21 cases. In all trajectories, repositioning involves twist-defect formation and propagation starting from the remodeler binding location, displaying only small deviations from those shown in Fig 4A.

Trajectories can be projected onto a low dimensional space defined by the sum of the contact indexes around the remodelers binding location ($\Delta b_{pL1} + \Delta b_{pL2} + \Delta b_{p1.5} + \Delta b_{p2.5}$, the horizontal axis in Fig 3B) and by the size of the twist defect around the dyad ($\Delta b_{p1.5} - \Delta b_{p-1.5}$, the vertical axis in Fig 4B). On this space, all the key metastable states involved in repositioning can be clearly separated (in Fig 4B we show trajectories 1 and 2 from panel a). From this figure we notice that most key conformational changes occur in the closed conformation (between two dotted lines). To test the importance of the system relaxation in this portion of the phase space, we induced ATP hydrolysis after only 10^6 MD steps from ATP binding (instead of 10^7). Even if limiting our analysis to the trajectories where the remodeler successfully closed before

hydrolysis (64%), only in 36% of the cases the remodeler can complete sliding by 1 bp, compared to the original 98% success rate (see [S1 Fig](#) for timeline of the contact indexes during one of these unsuccessful repositioning events). Failing to reposition occurs when the DNA does not have enough time to slide at the remodeler binding location (reaching state cD1), which is essential to avoid the steric overlap between lobe 2 and histones upon opening.

In [Fig 4C](#), we plot the changes in the average size of the twist defects at the SHLs near the remodeler during the ATP cycle. ATP binding and remodeler closure enhance the probabilities to find an extra base pair at SHL 1 and a missing base pair at SHL 2. Conversely, ATP hydrolysis and remodeler opening restore the former level of DNA twisting. Therefore, the closed remodeler lowers the free energy of opposite-type twist defects near its binding location at SHLs 1 and 2, which in turn will favor the initiation of DNA sliding towards the dyad starting from contact point 1.5, as observed in the trajectories in [Fig 4A](#).

Defect-mediated repositioning is controlled by DNA sequence

The twist-defect-mediated mechanism highlighted by our MD simulations may offer a further route to control the remodeling activity via DNA sequence (apart from the effects of positioning motifs described above), potentially explaining the significant sequence-dependence observed in experiments [[18,43,45,49,58,59](#)]. DNA sequence was already found to have a strong effect on the time-scales of spontaneous repositioning due to variations in DNA flexibility and energetics of twist defects [[49](#)]. When nucleosome diffusion is mediated by the formation of twist defects, repositioning proceeds much faster on sequences such as polyTpA, which are very flexible and easily accommodate twist defects, than on sequences such as poly(dA:dT) tracts (ApA repeats), which are stiffer and unlikely to display twist defects [[49](#)]. Perhaps surprisingly, it was shown that TpA repeats inhibit nucleosome repositioning by the Chd1 remodeler when the element is located at SHL 2 [[59](#)]. The origin of the influence of sequence on active repositioning is not clear, and there is likely also a strong dependence on the considered remodeler itself, due to the many different domains that can interact with the nucleosome apart from the translocase [[10](#)]. We begin exploring the defect-mediated sequence effects on the behavior of our minimal remodeler system by considering targeted changes from reference polyApG sequence at specific regions: the insertion of a 10-bp poly(dA:dT) tract at SHL 1 (polyApG-ApA_{SHL1} sequence), and a 10-bp TpA repeat at SHL 2 (polyApG-TpA_{SHL2} sequence) (see [Fig 5A](#) for the locations of these sequence elements within the Snf2-nucleosome complex). To characterize these effects, we reconstructed the free energy landscapes and kinetics of the systems via Markov state modeling [[70](#)] (the details on this analysis are given in the [S1 Text](#) and [S3 Fig](#)). In particular, we study the region of phase space where the translocase is in its closed (ATP-bound) configuration and lobe 1 fully completed the motion by 1 bp towards lobe 2, so that we can solely focus on the key formation and propagation of twist defects mediating repositioning.

In [Fig 5C](#), we display the free energy landscapes along the average contact index around SHL 2 (horizontal axis, $(\Delta bp_{1.5} + \Delta bp_{2.5})/2$, the same coordinate used to investigate sliding in [Fig 3](#)) and the number of twist defects at the three SHLs around the dyad (the vertical axis, $\Delta bp_{1.5} - \Delta bp_{-1.5}$, which enables to track how repositioning proceeds further away from SHL 2) for the three DNA sequences. These landscapes are qualitatively similar and have several local minima corresponding to the twist-defect intermediates observed in our trajectories. Indeed, the representative trajectories reported in [S2 Fig](#) (for 601, 5S rDNA, polyApG-ApA_{SHL1} and polyApG-TpA_{SHL2}) shows how the role of twist defects in mediating active repositioning is robust against changes in DNA sequence. However, the changes considered here do have significant effects on the kinetics of repositioning. For instance, if we focus on the pathway of twist-defect propagation observed in trajectory 2 in [Fig 4](#) (cB1 → cC2 → cD2 → cD1), which is

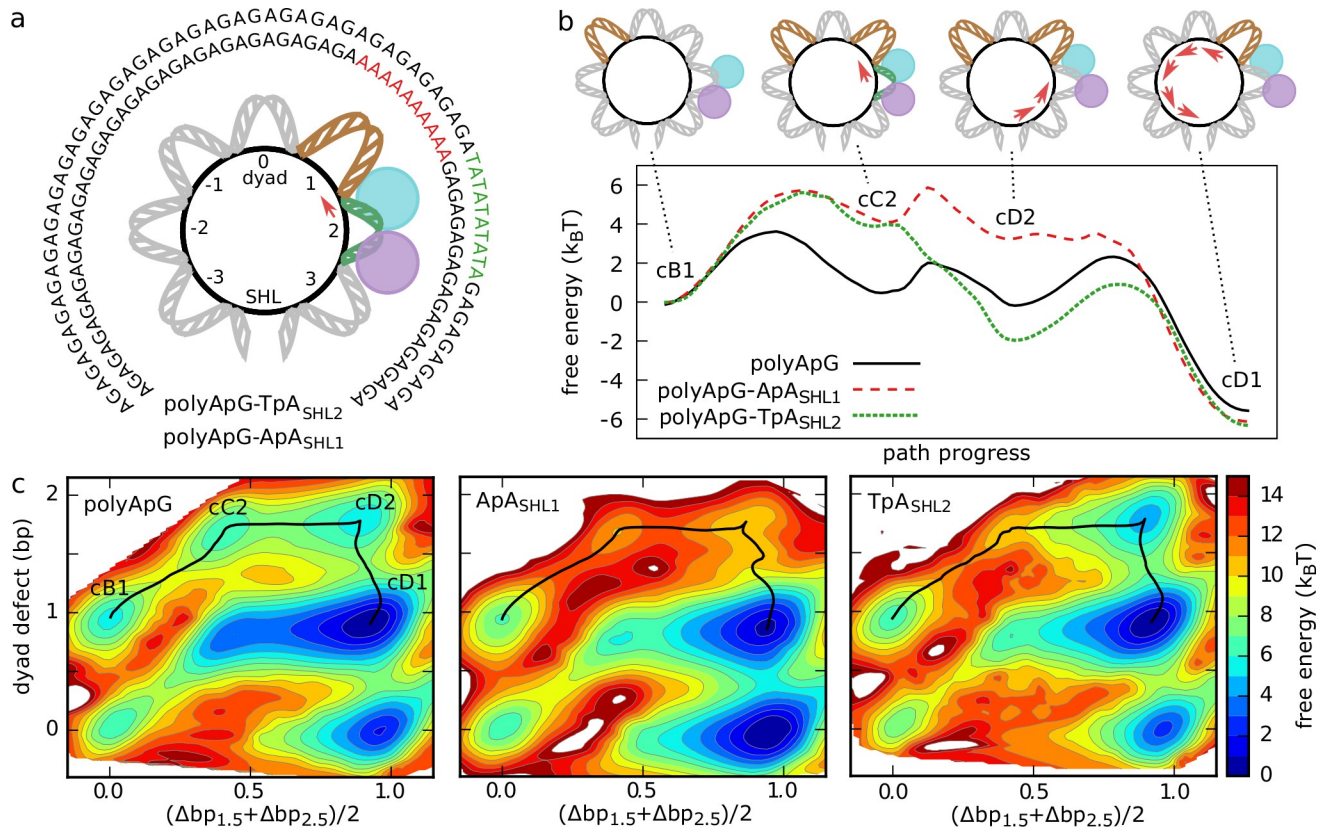


Fig 5. Twist-defect-mediated effects due to DNA sequence. (a) Considered DNA sequences apart from the reference polyApG: polyApG-ApA_{SHL1} (inner circle) and polyApG-TpA_{SHL2} (outer). We displayed the central 71 base pairs highlighting their location relative to the translocase-nucleosome complex. (b) Comparison of the free energy profiles along the minimum energy pathways of repositioning from state cB1 to state cD1; polyApG (black, solid line), polyApG-ApA_{SHL1} (red, dashed), and polyApG-TpA_{SHL2} (green, dotted). Errors on the profiles are within ~ 0.3 k_BT. (c) Free energy landscapes of the Snf2-nucleosome complex in the closed conformation along the average contact index at SHL 2, $(\Delta bp_{1.5} + \Delta bp_{2.5})/2$, and the size of the twist defects around the dyad $(\Delta bp_{1.5} - \Delta bp_{-1.5})$, for the three DNA sequences polyApG (left), polyApG-ApA_{SHL1} (center) and polyApG-TpA_{SHL2} (right). The minimum energy pathways are indicated on the landscapes by black solid lines.

<https://doi.org/10.1371/journal.pcbi.1006512.g005>

the most common for polyApG, highlighted in black in Fig 5C), then the addition of the ApA_{SHL1} and TpA_{SHL2} elements greatly increase the free energies of the intermediate states along the minimum energy pathways (Fig 5B). This effect is also evidenced by an increase in the mean first passage time to reach the final cD1 state (by a factor of ~ 2.4 and ~ 1.3 respectively). These changes are explained by the different DNA flexibilities and by the changes in defect pattern along the pathway of repositioning. ApA repeats were previously found to inhibit extra base pairs near the dyad, whereas TpA repeats were found to inhibit missing base pairs at SHLs ± 2 [49]. Since states cB1 and cD1 have only one defect around the dyad (at SHL +1 or -1), whereas the intermediate states cC2 and cD2 have two defects (at both SHLs +1 and -1), the ApA_{SHL1} element increases the free energy of these two intermediate states. Similarly, despite its flexibility, the TpA_{SHL2} element significantly increases the free energy of the cC2 state, where a missing base pair is accommodated at SHL 2. S1 Table summarizes the sequence dependence of the Snf2 activity on polyApG, 601, polyApG-ApA_{SHL1} and polyApG-TpA_{SHL2} nucleosomes. In all cases, variations from the reference uniform polyApG sequence have significant effects on the probability to induce repositioning, $(\Delta bp_{1.5} + \Delta bp_{2.5})/2 > 0.5$, at 10^7 MD steps after ATP binding, and/or on the mean first passage time to reach the final cD1 state.

Interestingly, we note that the repositioning activity may also depend on the DNA sequence at the translocase SHL 2 binding site via changes in the relative strength of lobe 1 and lobe 2 interactions with DNA. In particular, while the initial translocase closure occurring upon ATP binding always involves the motion of lobe 1 towards lobe 2 for polyApG, polyApG-ApA_{SHL1} and 601 Δ ₃, in ~28% of the polyApG-TpA_{SHL2} simulations lobe 2 moves towards lobe 1, due to the weaker lobe 2-DNA interactions. When this occurs, there is no sliding of nucleosomal DNA, since the original lobe 1 electrostatic interactions with SHL -6 remain unaffected, and the translocase opening following ATP hydrolysis simply brings the system back to its starting configuration. Therefore, our simulations suggest two possible explanations for the experimentally observed inhibitory effect of TpA repeats placed at SHL 2 [59]: either changes in the relative strength of the interactions between each lobe and DNA, or an increase in the free energy cost to generate twist-defect intermediates needed for repositioning (Fig 5B).

Discussion

The recent structural information of the Snf2-nucleosome complex [12] and insights from related molecular motors [36,37] allowed us to design an efficient computational model that reproduces the expected inchworm motion of the translocase domain along DNA [10]. More importantly, our MD simulations revealed the detailed molecular mechanism by which the inchworm motion of the translocase is converted into nucleosome repositioning. Specifically, we establish the fundamental role of electrostatic interactions and nucleosome twist defects. The interaction between a basic patch located on lobe 1 and the DNA gyre around SHL -6 acts as an electrostatic spring to direct the sliding of nucleosomal DNA from the translocase binding site at SHL 2 towards the dyad. Firstly, ATP binding drives the closure of the translocase via the motion of lobe 1 towards lobe 2 by 1 bp. This initial motion increases the distance between lobe 1 and SHL -6, weakening the electrostatic interactions. The sliding of nucleosomal DNA towards the dyad then causes the translocase to swing towards dyad together with DNA, re-establishing the original electrostatic contacts. The steric repulsion between the remodeler and the histone octamer allows nucleosomal DNA sliding to occur in the closed conformation only, and prevents sliding in the opposite direction away from the dyad. This mechanism is robust enough to enable active repositioning of nucleosomes formed with strong positioning sequences such as 601 [63], where sliding has to proceed against a high free-energy uphill due to the preferred rotational register of T/A positioning motifs. Consistent with previous experiments, our MD simulations of Snf2 mutants show that the basic patch on lobe 1 is essential for the ability to slide 601 nucleosomes [12].

The electrostatics-driven sliding of nucleosomal DNA starts from the histone-DNA contact point at SHL 1.5, via the formation of a pair of twist defects of opposite type at the neighboring SHLs: a -1bp defect at SHL 2 and a +1bp defect at SHL 1. The importance of twist defects lies in facilitating the initiation of nucleosomal DNA sliding locally from the translocase binding site, without simultaneously breaking distant histone-DNA contacts. The initial paired twist-defect conformation represents an intermediate state with tension accumulated around the remodeler location. Release of this tension via the propagation of the two twist defects in opposite directions completes the sliding of DNA by 1 bp throughout the entire nucleosome. The ATP cycle is completed after hydrolysis and ADP release, during which the motion of the weakened lobe 2 away from lobe 1 brings the translocase in the initial open conformation, only with the nucleosomal DNA slid by 1 bp relative to both histone octamer and remodeler. Interestingly, the twist defects that favor active nucleosome repositioning are the same that are commonly found in nucleosome crystal structures (at SHL 2) [1,31], and those that have been

shown to play an important role in spontaneous repositioning (SHL 1 and 2) [49], suggesting a reason for targeting the specific translocase binding location.

Our results are consistent with the wave-ratchet-wave model of nucleosome repositioning [10,32], where sliding is initiated at the translocase site via the generation of tension (DNA twisting). This has been suggested as a unifying fundamental mechanism of chromatin remodeling, where additional domains control tension release and interactions with other nucleosome regions to perform substrate recognition and to define the remodeling outcome (e.g. sliding vs histone ejection vs histone exchange) [10]. While we considered a minimal remodeler system consisting of nucleosome and translocase domain only, the molecular mechanism highlighted here may offer an understanding of more complex scenarios. For instance, the ISWI remodeler was found to slide nucleosomes via coordinated 3-bp entry and 1-bp exit steps [51]. These findings are consistent with our model if the additional HAND-SANT-SLIDE domain of ISWI blocks DNA sliding on the entry side until enough tension from twist defects is accumulated (3 bp), while on the exit side DNA sliding is unrestrained and it proceeds at 1-bp steps [10]. Although our computational model is currently not well tested for the study of histone conformational changes, the strong accumulation of tension from DNA twisting on the entry side may be related to the histone octamer distortions that are necessary for the remodeling activity of ISWI [40]. Distortions at the same histone regions have also been shown to contribute to thermally-driven nucleosome sliding [71], and their role deserves further investigation. Future studies should also address how remodelers may couple sliding of nucleosomal DNA to histone exchange [34].

Our simulations also reveal how the twist-defect mechanism allows a kinetic control of nucleosome repositioning via DNA sequence. This is due to the significant sequence-dependence in the formation of the twist-defect intermediates that facilitate repositioning. In our previous work [49], we showed how the free-energy cost of DNA twisting changes as a function of superhelical location (SHL) and sequence. With this knowledge, it is possible to target precise remodeling intermediates to control nucleosome sliding. Specifically, we tested the effect of introducing a 10-bp TpA repeat at SHL 2, which inhibits missing base pairs at this location, and a 10-bp poly(dA:dT) tract at SHL 1 (ApA_{SHL1}), which inhibits extra base pairs. Consistent with the important role of twist defects at these regions, both DNA sequence modifications slow-down sliding relative to the pure polyApG case, due to the increase in the free-energy barrier along the repositioning pathway. Notably, our TpA simulations explain recent experiments showing that the addition of this sequence element blocks repositioning by the Chd1 remodeler at SHL 2 [59]. These results may be considered surprising, because TpA base steps are known for their high flexibility [62] and expected to favor nucleosome sliding. Indeed, polyTpA sequences were found to be among those with the highest spontaneous nucleosome diffusivity [49]. However, even in that case, DNA sliding at SHL 2 represented the main kinetic bottleneck to sliding due to the high twist-defect cost [49], further supporting the tight relationship between spontaneous and active scenarios. Many experiments have also highlighted the role of poly(dA:dT) tracts in controlling remodeling outcomes [18,58,59]. Of note, while these sequences are well known for inhibiting their wrapping into nucleosomes [72], recent experiments suggested that the increase in the free energy of nucleosome assembly is not sufficient to explain the formation of nucleosome free regions [58], and that these are instead created via the direct action of chromatin remodelers [18,58]. Our molecular dynamics simulations reveal the detailed molecular mechanism by which DNA sequence changes affecting twist-defect formation may be exploited to control remodeling activities.

While this article was under review, an experimental work on the Chd1 remodeler by Winger et al. reported variations in the size of twist defects within the nucleosome as a function of the remodeler chemical state, suggesting that conformational changes in the translocase

may indeed stimulate the generation of twist defects necessary to slide nucleosomal DNA [73]. Further experimental studies evaluating the predictions of our simulations are very much needed. Finally, our computational methods may be readily employed for investigating the activity of different remodelers with known structural information, such as Chd1 [13] and INO80 [14,15], and for studying remodeling in the biologically-relevant context of a multi-nucleosome chromatin fiber [74].

Materials and methods

Our coarse-grained model employs the AICG2+ structure-based force field for proteins [60] and the 3SPN.2C force field for DNA [61]. This combination has been successfully applied in many past studies of nucleosome dynamics [9,43,45,49,54,55], and it enables a good compromise between computational speed-up and accuracy, necessary to reach the time-scales relevant to nucleosome repositioning [43,45,49]. According to these models, each amino acid is coarse-grained to a single bead located at the corresponding C α atom [60], whereas each nucleotide is represented by 3 beads corresponding to sugar, phosphate and base groups [61]. The reference native conformations of the histone octamer and the Snf2 ATPase are respectively taken from the nucleosome crystal structure with PDB id 1KX5 [65] and the nucleosome-Snf2 cryo-EM structure with PDB id 5X0Y [12]. Histone tails and remodeler disordered regions not visible in the reference structures are modeled according to a sequence-dependent local statistical potential [75]. The DNA model was parametrized against several experimental thermodynamic quantities, such as melting temperature, [61] and the sequence-dependent elasticity of DNA [62]. Notably, this model has been successfully employed to predict the role of DNA sequence on the free energy of nucleosome assembly [9] and the formation of twist defects [49], suggesting its suitability for investigating the sequence-dependent effects present in chromatin remodeling [18,58,59].

Histone octamer, remodeler and DNA interact via excluded volume, long-range electrostatics and hydrogen-bonds. For excluded volume, we employ bead-type dependent radii derived from a database of protein-protein and protein-DNA complexes [43,49,76]. Following our previous protocol [43,49], electrostatics is modeled according to Debye-Hückel theory, with standard unit charges placed on DNA phosphate groups and protein residues in flexible regions, and fractional charges on protein residue in folded regions derived using the RESPAC method, which optimizes the coarse-grained electrostatic potential against the all-atom one in the folded conformation [77]. For intra-DNA electrostatics, phosphate charges are rescaled by 0.6 to implicitly account for counter ion condensation [61]. In all simulations the salt concentration was set to 250 mM of monovalent ions. Histone-DNA hydrogen bonds are modeled using a recently-developed distance- and orientation-dependent potential between protein residues and phosphate groups [43,49]; the potential, unlike a Go-like contacts [54], is invariant under a rotation-coupled motion of DNA, allowing the study of nucleosome repositioning. These hydrogen bonds are defined from those observed in the 1KX5 [65] and 3LZ0 [78] crystal structures [43,49], and we employed the same hydrogen bond strength $\epsilon_{\text{HB}} = 1.8 k_{\text{B}}T$ used in Ref. [49], which is an intermediate value among those giving a nucleosome disassembly profile consistent with experiments [43]. Properly accounting for hydrogen-bond interactions is necessary for reproducing the experimental twist-defect metastability playing an important role in spontaneous nucleosome repositioning [47,49].

Translocase-DNA contacts are identified from the protein hydrogen donors within 5 Å from phosphate-group oxygen acceptors in the 5X0Y Snf2-nucleosome structure, and are represented with the same potential used for histone-DNA hydrogen bonds (reference distances and angles are also taken from 5X0Y). With this choice, lobe 1 (residue id 743–940) and lobe 2

(residue id 1046–1212) have each 16 contacts with DNA. These interactions are not strictly speaking only hydrogen bonds, but contacts introduced in the coarse-grained model to specify the remodeler-DNA binding mode. The relatively high cutoff is necessary to ensure that the motion of the remodeler lobes relative to the DNA occurs only during the translocase opening or closure steps induced during the ATP cycle, since spontaneous remodeler motion in the absence of ATP is inconsistent with the inchworm mechanism suggested from experiments [10,36,37]. The native reference structure of the open form of Snf2 corresponds to the cryo-EM structure with PDB id 5X0Y [12]. To model the remodeler in the closed conformation adopted upon ATP binding, we created additional lobe 1-lobe 2 Go-like contacts identified from the C α atoms within 7.5 Å in a homology model generated after aligning the two Snf2 lobes to the corresponding lobes found in the closed conformation of the NS3 helicase with PDB id 3KQU [37]. This reference structure was chosen because it was shown that the apo-state open conformations of Snf2 [12] (PDB id 5X0Y) and NS3 [37] (PDB id 3KQH) display a high degree of structural similarity [12]. These additional lobe 1-lobe 2 contacts take the standard Lennard-Jones form with 10–12 exponents that is employed by the AICG2+ model for native contacts [60]. To simulate the conformational change between the open and closed forms of Snf2, we change the strength of the lobe 1-lobe 2 contacts during the simulation: when the contacts are weak, these do not form and Snf2 preferentially adopts the main reference open conformation found in the 5X0Y cryo-EM structure; when the contacts are strong, lobes 1 and 2 becomes closer and the translocase adopts a conformation similar to the one of the closed NS3 helicase [37] (see next paragraph for details on the changes in contact strengths during the ATP cycle).

As described at the beginning of the Results section, we simulate the remodeling activity of Snf2 during a full ATP cycle by switching the underlying potential to model changes in the translocase chemical state, as previously done for modeling other protein motors [57,64]. The key elements of our Snf2 model are based on well-established experimental observations for many DNA translocases; specifically, the conformational change from an open to a closed conformation upon ATP binding [12,13,36], and the weakening of lobe 2 interactions with DNA relative to those of lobe 1 upon ATP hydrolysis [37]. The free parameters in our model are simply chosen to satisfy these reasonable assumptions. Each MD simulation cycle consists of 2×10^7 MD equilibration steps in the apo-state, 10^7 steps in the ATP-bound state, and 10^7 steps in the ADP-bound state. In the apo state, translocase-DNA contacts have the same strength as histone-DNA hydrogen bonds ($\epsilon_{1\text{-DNA}} = \epsilon_{2\text{-DNA}} = 1.8 \text{ k}_B\text{T}$) and lobe 1-lobe 2 contacts are very weak ($\epsilon_{1\text{-}2} = 0.17 \text{ k}_B\text{T}$), so that the other native interactions based on the 5X0Y reference dominate and the translocase is preferably in its open conformation. In the ATP-bound state, translocase-DNA interactions remain unchanged, but the interactions between lobe 1 and lobe 2 are strengthened ($\epsilon_{1\text{-}2} = 1.0 \text{ k}_B\text{T}$) to stabilize the closed conformation. After ATP hydrolysis, lobe 2-DNA interactions are weakened by a factor of 0.8 ($\epsilon_{2\text{-DNA}} = 1.44 \text{ k}_B\text{T}$). Completing the cycle requires a last switch to the apo-state potential, but this only changes the translocase-DNA interactions, without inducing any conformational change. With these settings, we generate with very high probability successful nucleosome repositioning by 1 bp in the correct direction [12] (DNA sliding from the remodeler site towards the dyad, see Results section) via the inchworm mechanism suggested from past experimental studies [10,36,37]. Variations to this simulation protocol, such as using the recent nucleosome-Chd1 cryo-EM structure to model the ATP-bound closed conformation [13] or changes to the Snf2-DNA interactions, have been also tested, but they do not affect the key features of the active repositioning mechanism mediated by twist defects presented in the Results section.

MD simulations have been performed using the software CafeMol 3.0 [79] (available at <http://www.cafemol.org/>), integrating the equations of motion using the default settings via Langevin dynamics at 300 K. For the cases where the remodeler is in complex with the

nucleosome, we ran 100 MD simulation cycles for each system, whereas for the remodeler sliding on naked DNA we ran 40 cycles. In the former cases, nucleosomal DNA is made by 223 bp (central 147 bp plus 38 bp for each linker), whereas in the latter by 40 bp. Nucleosome-bound simulations start from the conformation observed in the 5X0Y structure [12] after a short energy minimization with the steepest descent method (Fig 1C). In the S1 Text we provide details on the generation of the free-energy landscapes and kinetics of the systems from our MD trajectories via Markov state modeling [70].

Supporting information

S1 Text. Supplementary methods describing the details of our free-energy calculations and Markov state modeling.

(PDF)

S1 Fig. Unsuccessful repositioning. Timeline of the translocase (L1 and L2) and nucleosome contact indexes (SHL -4.5 to 4.5) for a representative trajectory where ATP consumption does not induce nucleosome sliding. ATP binding occurs at time 0, inducing the closure of the remodeler after about 0.5×10^6 MD steps. Here we induce ATP hydrolysis only after 10^6 MD steps (instead of 10^7), so that the remodeler does not have enough time to induce sliding of nucleosomal DNA before the opening of the ATPase domain, which simply causes the system to come back to the initial open conformation because of steric interactions between lobe 2 (in purple) and the nucleosome.

(TIF)

S2 Fig. Active nucleosome repositioning via twist-defect propagation on different nucleosomal DNA sequences: (a) 601, (b) 5S rDNA, (c) polyApG-ApA_{SHL1}, and (d) polyApG-TpA_{SHL2}. We show timelines of the translocase (L1 and L2) and nucleosome contact indexes (SHL -4.5 to 4.5) for representative trajectories where nucleosomal DNA slides by 1 bp relative to the initial configuration. As in Fig 4A from the main text, these plots highlight how nucleosome repositioning occurs via the formation and propagation of twist defects from the remodeler binding location at SHL 2.

(TIF)

S3 Fig. Relaxation time scales from Markov state modeling. For each considered system, we plot the four slowest relaxation time scales of the MSM as a function of the chosen lag-time. The results reported in the main text were obtained with a lag-time of 2.5×10^5 MD steps (indicated by the vertical dotted lines), after which the time scales are nearly constant.

(TIF)

S1 Table. Summary of the sequence dependence of the Snf2 activity on polyApG, 601, polyApG-ApA_{SHL1} and polyApG-TpA_{SHL2} nucleosomes, showing the probability to induce repositioning, $(\Delta bp_{1.5} + \Delta bp_{2.5})/2 > 0.5$, at 10^7 MD steps after ATP binding (P_sliding), the mean first passage time to reach the final repositioned cD1 state (T_sliding), and the total number of MD trajectories run for each sequence.

(TIF)

S1 Movie. Snf2 inchworm motion on naked DNA. Snapshots taken from a representative trajectory of the translocase sliding on naked DNA during an ATP cycle. Lobe 1 is shown in cyan, lobe 2 in purple and DNA in gray. In yellow we display two reference phosphate groups to highlight the inchworm motion of the lobes relative to the DNA. First, ATP binding induces the translocase closure, with the motion of lobe 1 towards lobe 2. Second, ATP hydrolysis weakens the lobe 2-DNA interactions and induces the translocase opening, with the motion of

lobe 2 away from lobe 1.
(MPG)

S2 Movie. Coupling between Snf2 inchworm motion and nucleosome sliding. Snapshots of trajectory 1 in Fig 4A from the main text, focusing on how the translocase inchworm motion during the ATP cycle is coupled to sliding of nucleosomal DNA at the SHL 2 binding site. Lobe 1 as shown in the cyan transparency, lobe 2 in the purple transparency, DNA in gray, histones H3 in pink, H4 in orange, H2A and H2B in light and dark green respectively. To highlight the key motions of the system, we depict as larger beads a reference residue on lobe 1 (in cyan), a residue on lobe 2 (purple), and one DNA phosphate per turn (red, corresponding to the histone-DNA contact points). We also show as smaller brown beads the K855, R880 and K885 residues on lobe 1 mediating the electrostatic interactions with the DNA gyre at SHL -6. At the beginning of the movie we see the ATP-driven translocase closure with the motion of lobe 1 towards lobe 2 (after ~2 seconds in the movie, $\sim 0.03 \times 10^6$ MD steps in the simulation). Then nucleosomal DNA slides around SHL 2 towards the dyad (note the counter-clockwise motion of two phosphates near the remodeler between ~8 and ~12 seconds in the movie, $\sim 0.13 \times 10^6$ to $\sim 0.2 \times 10^6$ MD steps). Finally, ATP hydrolysis induces the translocase opening with the motion of lobe 2 away from lobe 1 (~14 seconds in the movie, $\sim 10^7$ MD steps). As in Fig 4A of the main text, part of the trajectory (during which no key motions occur) is omitted for clarity.
(MPG)

S3 Movie. Nucleosome repositioning via twist defects. Snapshots of the same trajectory 1 in Fig 4A from the main text represented in S2 Movie, but now focusing on DNA sliding throughout the entire nucleosome via twist defects. Lobe 1 as shown in the cyan transparency, lobe 2 in the purple transparency, DNA in gray, histones H3 in pink, H4 in orange, H2A and H2B in light and dark green respectively. To highlight the key motions of the system, we depict as larger beads a reference residue on lobe 1 (in cyan), a residue on lobe 2 (purple), and one DNA phosphate per turn (red, corresponding to the histone-DNA contact points). At the beginning of the movie we see the ATP-driven translocase closure with the motion of lobe 1 towards lobe 2 (after ~2 seconds in the movie, $\sim 0.03 \times 10^6$ MD steps in the simulation). Then we see sliding of nucleosomal DNA at the contact point at SHL 1.5 towards the dyad (note the motion of the 3rd phosphate group, counting counter-clockwise, at ~8 seconds in the movie, $\sim 0.13 \times 10^6$ MD steps), with the generation of a +1bp defect at SHL 1 and a -1bp twist defect at SHL 2. At ~12 seconds in the movie ($\sim 0.2 \times 10^6$ MD steps) we see the motion of nucleosomal DNA at contact points 2.5 and 3.5 (note the 1st and 2nd phosphates), releasing the -1bp defect at SHL 2. Then ATP hydrolysis induces the opening of the translocase and the motion of lobe 2 away from lobe 1 (~14 seconds in the movie, $\sim 10^7$ MD steps). Finally, the motion of nucleosomal DNA at the remaining contact points (note the phosphates near SHL 0.5, -0.5, -1.5 and -2.5), completes repositioning of the nucleosome (~17 seconds in the movie, $\sim 18 \times 10^7$ MD steps), releasing the extra base pair at SHL 1.
(MPG)

Acknowledgments

We thank Ralf Blossey for stimulating discussions on chromatin remodeling mechanisms. We are also grateful to Tsuyoshi Terakawa for carefully reading our manuscript.

Author Contributions

Conceptualization: Giovanni B. Brandani.

Data curation: Giovanni B. Brandani.
Formal analysis: Giovanni B. Brandani.
Funding acquisition: Shoji Takada.
Investigation: Giovanni B. Brandani.
Methodology: Giovanni B. Brandani.
Project administration: Shoji Takada.
Resources: Shoji Takada.
Software: Giovanni B. Brandani, Shoji Takada.
Supervision: Shoji Takada.
Validation: Giovanni B. Brandani, Shoji Takada.
Visualization: Giovanni B. Brandani.
Writing – original draft: Giovanni B. Brandani.
Writing – review & editing: Giovanni B. Brandani, Shoji Takada.

References

1. Richmond TJ, Davey CA. The structure of DNA in the nucleosome core. *Nature*. Nature Publishing Group; 2003; 423: 145–150. <https://doi.org/10.1038/nature01595> PMID: 12736678
2. Lai WKM, Pugh BF. Understanding nucleosome dynamics and their links to gene expression and DNA replication. *Nat Rev Mol Cell Biol*. Nature Publishing Group; 2017; 18: 548–562. <https://doi.org/10.1038/nrm.2017.47> PMID: 28537572
3. Field Y, Kaplan N, Fondufe-Mittendorf Y, Moore IK, Sharon E, Lubling Y, et al. Distinct Modes of Regulation by Chromatin Encoded through Nucleosome Positioning Signals. Ohler U, editor. *PLoS Comput Biol*. Public Library of Science; 2008; 4: e1000216. <https://doi.org/10.1371/journal.pcbi.1000216> PMID: 18989395
4. Struhl K, Segal E. Determinants of nucleosome positioning. *Nat Struct Mol Biol*. 2013; 20: 267–273. <https://doi.org/10.1038/nsmb.2506> PMID: 23463311
5. Teif VB, Vainshtein Y, Caudron-Herger M, Mallm J-P, Marth C, Höfer T, et al. Genome-wide nucleosome positioning during embryonic stem cell development. *Nat Struct Mol Biol*. Nature Publishing Group; 2012; 19: 1185–1192. <https://doi.org/10.1038/nsmb.2419> PMID: 23085715
6. Shivaswamy S, Bhingre A, Zhao Y, Jones S, Hirst M, Iyer VR. Dynamic Remodeling of Individual Nucleosomes Across a Eukaryotic Genome in Response to Transcriptional Perturbation. *PLoS Biol*. Public Library of Science; 2008; 6: e65. <https://doi.org/10.1371/journal.pbio.0060065> PMID: 18351804
7. Reja R, Vinayachandran V, Ghosh S, Pugh BF. Molecular mechanisms of ribosomal protein gene coregulation. *Genes Dev*. Cold Spring Harbor Laboratory Press; 2015; 29: 1942–54. <https://doi.org/10.1101/gad.268896.115> PMID: 26385964
8. Morozov A V, Fortney K, Gaykalova DA, Studitsky VM, Widom J, Siggia ED. Using DNA mechanics to predict in vitro nucleosome positions and formation energies. *Nucleic Acids Res*. 2009; 37: 4707–4722. <https://doi.org/10.1093/nar/gkp475> PMID: 19509309
9. Freeman GS, Lequieu JP, Hinckley DM, Whitmer JK, de Pablo JJ. DNA Shape Dominates Sequence Affinity in Nucleosome Formation. *Phys Rev Lett*. 2014; 113: 168101. <https://doi.org/10.1103/PhysRevLett.113.168101> PMID: 25361282
10. Clapier CR, Iwasa J, Cairns BR, Peterson CL. Mechanisms of action and regulation of ATP-dependent chromatin-remodelling complexes. *Nat Rev Mol Cell Biol*. 2017; 18: 407–422. <https://doi.org/10.1038/nrm.2017.26> PMID: 28512350
11. Zhou CY, Johnson SL, Gamarra NI, Narlikar GJ. Mechanisms of ATP-Dependent Chromatin Remodeling Motors. *Annu Rev Biophys*. Annual Reviews; 2016; 45: 153–181. <https://doi.org/10.1146/annurev-biophys-051013-022819> PMID: 27391925
12. Liu X, Li M, Xia X, Li X, Chen Z. Mechanism of chromatin remodelling revealed by the Snf2-nucleosome structure. *Nature*. Nature Publishing Group; 2017; 544: 440–445. <https://doi.org/10.1038/nature22036> PMID: 28424519

13. Farnung L, Vos SM, Wigge C, Cramer P. Nucleosome–Chd1 structure and implications for chromatin remodelling. *Nature*. Nature Publishing Group; 2017; 550: 539. <https://doi.org/10.1038/nature24046> PMID: 29019976
14. Ayala R, Willhoft O, Aramayo RJ, Wilkinson M, McCormack EA, Ocloo L, et al. Structure and regulation of the human INO80–nucleosome complex. *Nature*. Nature Publishing Group; 2018; 556: 391–395. <https://doi.org/10.1038/s41586-018-0021-6> PMID: 29643506
15. Eustermann S, Schall K, Kostrewa D, Lakomek K, Strauss M, Moldt M, et al. Structural basis for ATP-dependent chromatin remodelling by the INO80 complex. *Nature*. Nature Publishing Group; 2018; 556: 386–390. <https://doi.org/10.1038/s41586-018-0029-y> PMID: 29643509
16. Torigoe E. S, Urwin DL, Ishii H, Smith DE, Kadonaga JT. Identification of a Rapidly Formed Nonnucleosomal Histone-DNA Intermediate that Is Converted into Chromatin by ACF. *Mol Cell*. Cell Press; 2011; 43: 638–648. <https://doi.org/10.1016/j.molcel.2011.07.017> PMID: 21855802
17. Gkikopoulos T, Schofield P, Singh V, Pinskaya M, Mellor J, Smolle M, et al. A Role for Snf2-Related Nucleosome-Spacing Enzymes in Genome-Wide Nucleosome Organization. *Science*. 2011; 333: 1758–1760. <https://doi.org/10.1126/science.1206097> PMID: 21940898
18. Krietenstein N, Wal M, Watanabe S, Park B, Peterson CL, Pugh BF, et al. Genomic Nucleosome Organization Reconstituted with Pure Proteins. *Cell*. Cell Press; 2016; 167: 709–721.e12. <https://doi.org/10.1016/j.cell.2016.09.045> PMID: 27768892
19. Yang JG, Madrid TS, Sevastopoulos E, Narlikar GJ. The chromatin-remodeling enzyme ACF is an ATP-dependent DNA length sensor that regulates nucleosome spacing. *Nat Struct Mol Biol*. 2006; 13: 1078–1083. <https://doi.org/10.1038/nsmb1170> PMID: 17099699
20. Harada BT, Hwang WL, Deindl S, Chatterjee N, Bartholomew B, Zhuang X, et al. Stepwise nucleosome translocation by RSC remodeling complexes. *Elife*. eLife Sciences Publications; 2016; 5: 339–346. <https://doi.org/10.7554/eLife.10051> PMID: 26895087
21. Boeger H, Griesenbeck J, Strattan JS, Kornberg RD. Removal of Promoter Nucleosomes by Disassembly Rather Than Sliding In Vivo. *Mol Cell*. Cell Press; 2004; 14: 667–673. <https://doi.org/10.1016/j.molcel.2004.05.013> PMID: 15175161
22. Bruno M, Flaus A, Stockdale C, Rencurel C, Ferreira H, Owen-Hughes T. Histone H2A/H2B Dimer Exchange by ATP-Dependent Chromatin Remodeling Activities. *Mol Cell*. Cell Press; 2003; 12: 1599–1606. [https://doi.org/10.1016/S1097-2765\(03\)00499-4](https://doi.org/10.1016/S1097-2765(03)00499-4) PMID: 14690611
23. Vasseur P, Tonazzini S, Ziane R, Camasses A, Rando OJ, Radman-Livaja M. Dynamics of Nucleosome Positioning Maturation following Genomic Replication. *Cell Rep*. Cell Press; 2016; 16: 2651–2665. <https://doi.org/10.1016/j.celrep.2016.07.083> PMID: 27568571
24. Lorch Y, Kornberg RD. Chromatin-remodeling and the initiation of transcription. *Q Rev Biophys*. Cambridge University Press; 2015; 48: 465–470. <https://doi.org/10.1017/S0033583515000116> PMID: 26537406
25. Schones DE, Cui K, Cuddapah S, Roh T-Y, Barski A, Wang Z, et al. Dynamic Regulation of Nucleosome Positioning in the Human Genome. *Cell*. Cell Press; 2008; 132: 887–898. <https://doi.org/10.1016/j.cell.2008.02.022> PMID: 18329373
26. Mueller-Planitz F, Klinker H, Becker PB. Nucleosome sliding mechanisms: new twists in a looped history. *Nat Struct Mol Biol*. Nature Publishing Group; 2013; 20: 1026–32. <https://doi.org/10.1038/nsmb.2648> PMID: 24008565
27. Flaus A, Owen-Hughes T. Mechanisms for ATP-dependent chromatin remodelling: the means to the end. *FEBS J*. Blackwell Publishing Ltd; 2011; 278: 3579–3595. <https://doi.org/10.1111/j.1742-4658.2011.08281.x> PMID: 21810178
28. Blossey R, Schiessel H. Kinetic proofreading of gene activation by chromatin remodeling. *HFSP J*. Taylor & Francis Group; 2008; 2: 167–170. <https://doi.org/10.2976/1.2909080> PMID: 19404470
29. Narlikar GJ. A proposal for kinetic proof reading by ISWI family chromatin remodeling motors. *Curr Opin Chem Biol*. Elsevier Current Trends; 2010; 14: 660–665. <https://doi.org/10.1016/j.cbpa.2010.08.001> PMID: 20833099
30. Zofall M, Persinger J, Kassabov SR, Bartholomew B. Chromatin remodeling by ISW2 and SWI/SNF requires DNA translocation inside the nucleosome. *Nat Struct Mol Biol*. Nature Publishing Group; 2006; 13: 339–346. <https://doi.org/10.1038/nsmb1071> PMID: 16518397
31. Luger K, Mäder AW, Richmond RK, Sargent DF, Richmond TJ. Crystal structure of the nucleosome core particle at 2.8 Å resolution. *Nature*. 1997; 389: 251–260. <https://doi.org/10.1038/38444> PMID: 9305837
32. Saha A, Wittmeyer J, Cairns BR. Chromatin remodeling through directional DNA translocation from an internal nucleosomal site. *Nat Struct Mol Biol*. Nature Publishing Group; 2005; 12: 747–755. <https://doi.org/10.1038/nsmb973> PMID: 16086025

33. Schwanbeck R, Xiao H, Wu C. Spatial contacts and nucleosome step movements induced by the NURF chromatin remodeling complex. *J Biol Chem. American Society for Biochemistry and Molecular Biology*; 2004; 279: 39933–41. <https://doi.org/10.1074/jbc.M406060200> PMID: 15262970
34. Brahma S, Udugama MI, Kim J, Hada A, Bhardwaj SK, Hailu SG, et al. INO80 exchanges H2A.Z for H2A by translocating on DNA proximal to histone dimers. *Nat Commun. Nature Publishing Group*; 2017; 8: 15616. <https://doi.org/10.1038/ncomms15616> PMID: 28604691
35. Patel A, Chakravarthy S, Morrone S, Nodelman IM, McKnight JN, Bowman GD. Decoupling nucleosome recognition from DNA binding dramatically alters the properties of the Chd1 chromatin remodeler. *Nucleic Acids Res. Oxford University Press*; 2013; 41: 1637–1648. <https://doi.org/10.1093/nar/gks1440> PMID: 23275572
36. Velankar SS, Soultanas P, Dillingham MS, Subramanya HS, Wigley DB. Crystal Structures of Complexes of PcrA DNA Helicase with a DNA Substrate Indicate an Inchworm Mechanism. *Cell. Cell Press*; 1999; 97: 75–84. [https://doi.org/10.1016/S0092-8674\(00\)80716-3](https://doi.org/10.1016/S0092-8674(00)80716-3) PMID: 10199404
37. Gu M, Rice CM. Three conformational snapshots of the hepatitis C virus NS3 helicase reveal a ratchet translocation mechanism. *Proc Natl Acad Sci U S A. National Academy of Sciences*; 2010; 107: 521–8. <https://doi.org/10.1073/pnas.0913380107> PMID: 20080715
38. Sirinakis G, Clapier CR, Gao Y, Viswanathan R, Cairns BR, Zhang Y. The RSC chromatin remodelling ATPase translocates DNA with high force and small step size. *EMBO J. European Molecular Biology Organization*; 2011; 30: 2364–72. <https://doi.org/10.1038/emboj.2011.141> PMID: 21552204
39. Zhang Y, Smith CL, Saha A, Grill SW, Mihardja S, Smith SB, et al. DNA Translocation and Loop Formation Mechanism of Chromatin Remodeling by SWI/SNF and RSC. *Mol Cell. Cell Press*; 2006; 24: 559–568. <https://doi.org/10.1016/j.molcel.2006.10.025> PMID: 17188033
40. Sinha KK, Gross JD, Narlikar GJ. Distortion of histone octamer core promotes nucleosome mobilization by a chromatin remodeler. *Science*. 2017; 355: eaaa3761. <https://doi.org/10.1126/science.aaa3761> PMID: 28104838
41. Blossey R, Schiessel H. The dynamics of the nucleosome: thermal effects, external forces and ATP. *FEBS J. Blackwell Publishing Ltd*; 2011; 278: 3619–3632. <https://doi.org/10.1111/j.1742-4658.2011.08283.x> PMID: 21812931
42. Meersseman G, Pennings S, Bradbury EM. Mobile nucleosomes—a general behavior. *EMBO J. European Molecular Biology Organization*; 1992; 11: 2951–2959. Available: <http://www.ncbi.nlm.nih.gov/pubmed/1639066> PMID: 1639066
43. Niina T, Brandani GB, Tan C, Takada S. Sequence-dependent nucleosome sliding in rotation-coupled and uncoupled modes revealed by molecular simulations. Panchenko ARR, editor. *PLOS Comput Biol. Public Library of Science*; 2017; 13: e1005880. <https://doi.org/10.1371/journal.pcbi.1005880> PMID: 29194442
44. Schiessel H, Widom J, Bruinsma RF, Gelbart WM. Polymer Reptation and Nucleosome Repositioning. *Phys Rev Lett*. 2001; 86: 4414–4417. <https://doi.org/10.1103/PhysRevLett.86.4414> PMID: 11328188
45. Lequieu J, Schwartz DC, de Pablo JJ. In silico evidence for sequence-dependent nucleosome sliding. *Proc Natl Acad Sci U S A*. 2017; 44: E9197–E9205. <https://doi.org/10.1073/pnas.1705685114>
46. van Holde KE, Yager TD. Nucleosome Motion: Evidence and Models. *Structure and Function of the Genetic Apparatus*. Boston, MA: Springer US; 1985. pp. 35–53. https://doi.org/10.1007/978-1-4684-5024-8_4
47. Kulić IM, Schiessel H. Chromatin Dynamics: Nucleosomes go Mobile through Twist Defects. *Phys Rev Lett*. 2003; 91: 148103. <https://doi.org/10.1103/PhysRevLett.91.148103> PMID: 14611559
48. Edayathumangalam RS, Weyermann P, Dervan PB, Gottesfeld JM, Luger K. Nucleosomes in Solution Exist as a Mixture of Twist-defect States. *J Mol Biol*. 2005; 345: 103–114. <https://doi.org/10.1016/j.jmb.2004.10.012> PMID: 15567414
49. Brandani GB, Niina T, Tan C, Takada S. DNA sliding in nucleosomes via twist defect propagation revealed by molecular simulations. *Nucleic Acids Res. Oxford University Press*; 2018; 46: 2788–2801. <https://doi.org/10.1093/nar/gky158> PMID: 29506273
50. Shaytan AK, Armeev GA, Goncareenco A, Zhurkin VB, Landsman D, Panchenko AR. Coupling between Histone Conformations and DNA Geometry in Nucleosomes on a Microsecond Timescale: Atomistic Insights into Nucleosome Functions. *J Mol Biol*. 2016; 428: 221–237. <https://doi.org/10.1016/j.jmb.2015.12.004> PMID: 26699921
51. Deindl Sebastian, Hwang WL, Hota SK, Blosser TR, Prasad P, et al. ISWI remodelers slide nucleosomes with coordinated multi-base-pair entry steps and single-base-pair exit steps. *Cell. Cell Press*; 2013; 152: 442–452. <https://doi.org/10.1016/j.cell.2012.12.040> PMID: 23374341
52. Takada S, Kanada R, Tan C, Terakawa T, Li W, Kenzaki H. Modeling Structural Dynamics of Biomolecular Complexes by Coarse-Grained Molecular Simulations. *Acc Chem Res*. 2015; 48: 3026–3035. <https://doi.org/10.1021/acs.accounts.5b00338> PMID: 26575522

53. Flechsig H, Mikhailov AS. Tracing entire operation cycles of molecular motor hepatitis C virus helicase in structurally resolved dynamical simulations. *Proc Natl Acad Sci U S A. National Academy of Sciences*; 2010; 107: 20875–80. <https://doi.org/10.1073/pnas.1014631107> PMID: 21081697
54. Kenzaki H, Takada S. Partial Unwrapping and Histone Tail Dynamics in Nucleosome Revealed by Coarse-Grained Molecular Simulations. *PLoS Comput Biol*. 2015; 11: e1004443. <https://doi.org/10.1371/journal.pcbi.1004443> PMID: 26262925
55. Chang L, Takada S. Histone acetylation dependent energy landscapes in tri-nucleosome revealed by residue-resolved molecular simulations. *Sci Rep*. 2016; 6: 34441. <https://doi.org/10.1038/srep34441> PMID: 27698366
56. Zhang B, Zheng W, Papoian GA, Wolynes PG. Exploring the Free Energy Landscape of Nucleosomes. *J Am Chem Soc*. 2016; 138: 8126–8133. <https://doi.org/10.1021/jacs.6b02893> PMID: 27300314
57. Koga N, Takada S. Folding-based molecular simulations reveal mechanisms of the rotary motor F1–ATPase. *Proc Natl Acad Sci U S A*. 2006; 103: 5367–5372. Available: <http://www.pnas.org/content/pnas/103/14/5367.full.pdf> <https://doi.org/10.1073/pnas.0509642103> PMID: 16567655
58. Lorch Y, Maier-Davis B, Kornberg RD. Role of DNA sequence in chromatin remodeling and the formation of nucleosome-free regions. *Genes Dev. Cold Spring Harbor Laboratory Press*; 2014; 28: 2492–7. <https://doi.org/10.1101/gad.250704.114> PMID: 25403179
59. Winger J, Bowman GD. The Sequence of Nucleosomal DNA Modulates Sliding by the Chd1 Chromatin Remodeler. *J Mol Biol. Academic Press*; 2017; 429: 808–822. <https://doi.org/10.1016/j.jmb.2017.02.002> PMID: 28189426
60. Li W, Wang W, Takada S. Energy landscape views for interplays among folding, binding, and allostery of calmodulin domains. *Proc Natl Acad Sci U S A*. 2014; 111: 10550–10555. <https://doi.org/10.1073/pnas.1402768111> PMID: 25002491
61. Freeman GS, Hinckley DM, Lequieu JP, Whitmer JK, de Pablo JJ. Coarse-grained modeling of DNA curvature. *J Chem Phys*. 2014; 141: 165103. <https://doi.org/10.1063/1.4897649> PMID: 25362344
62. Olson WK, Gorin AA, Lu XJ, Hock LM, Zhurkin VB. DNA sequence-dependent deformability deduced from protein-DNA crystal complexes. *Proc Natl Acad Sci U S A*. 1998; 95: 11163–11168. <https://doi.org/10.1073/PNAS.95.19.11163> PMID: 9736707
63. Lowary P., Widom J. New DNA sequence rules for high affinity binding to histone octamer and sequence-directed nucleosome positioning. *J Mol Biol*. 1998; 276: 19–42. <https://doi.org/10.1006/jmbi.1997.1494> PMID: 9514715
64. Yao X-Q, Kenzaki H, Murakami S, Takada S. Drug export and allosteric coupling in a multidrug transporter revealed by molecular simulations. *Nat Commun. Nature Publishing Group, a division of Macmillan Publishers Limited. All Rights Reserved.*; 2010; 1: 117. <https://doi.org/10.1038/ncomms1116> PMID: 21081915
65. Davey CA, Sargent DF, Luger K, Maeder AW, Richmond TJ. Solvent Mediated Interactions in the Structure of the Nucleosome Core Particle at 1.9Å Resolution. *J Mol Biol*. 2002; 319: 1097–1113. [https://doi.org/10.1016/S0022-2836\(02\)00386-8](https://doi.org/10.1016/S0022-2836(02)00386-8) PMID: 12079350
66. Richmond TJ, Widom J. Nucleosome and chromatin structure. *Chromatin structure and gene expression. Oxford University Press Oxford, UK*; 2000. pp. 1–19.
67. Jülicher F, Ajdari A, Prost J. Modeling molecular motors. *Rev Mod Phys. American Physical Society*; 1997; 69: 1269–1282. <https://doi.org/10.1103/RevModPhys.69.1269>
68. Flaus A, Luger K, Tan S, Richmond TJ. Mapping nucleosome position at single base-pair resolution by using site-directed hydroxyl radicals. *Proc Natl Acad Sci U S A. National Academy of Sciences*; 1996; 93: 1370–5. <https://doi.org/10.1073/PNAS.93.4.1370> PMID: 8643638
69. van der Heijden T, van Vugt JJFA, Logie C, van Noort J. Sequence-based prediction of single nucleosome positioning and genome-wide nucleosome occupancy. *Proc Natl Acad Sci U S A. National Academy of Sciences*; 2012; 109: E2514–22. <https://doi.org/10.1073/pnas.1205659109> PMID: 22908247
70. Prinz J-H, Wu H, Sarich M, Keller B, Senne M, Held M, et al. Markov models of molecular kinetics: Generation and validation. *J Chem Phys*. 2011; 134: 174105. <https://doi.org/10.1063/1.3565032> PMID: 21548671
71. Bilokapic S, Strauss M, Halic M. Structural rearrangements of the histone octamer translocate DNA. *Nat Commun. Nature Publishing Group*; 2018; 9: 1330. <https://doi.org/10.1038/s41467-018-03677-z> PMID: 29626188
72. Segal E, Widom J. Poly(dA:dT) tracts: major determinants of nucleosome organization. *Curr Opin Struct Biol*. 2009; 19: 65–71. <https://doi.org/10.1016/j.sbi.2009.01.004> PMID: 19208466
73. Winger J, Nodelman IM, Levandosky RF, Bowman GD. A twist defect mechanism for ATP-dependent translocation of nucleosomal DNA. *Elife. eLife Sciences Publications Limited*; 2018; 7: e34100. <https://doi.org/10.7554/eLife.34100> PMID: 29809147

74. Nikitina T, Norouzi D, Grigoryev SA, Zhurkin VB. DNA topology in chromatin is defined by nucleosome spacing. *Sci Adv. American Association for the Advancement of Science*; 2017; 3: e1700957. <https://doi.org/10.1126/sciadv.1700957> PMID: 29098179
75. Terakawa T, Takada S. Multiscale ensemble modeling of intrinsically disordered proteins: p53 N-terminal domain. *Biophys J*. 2011; 101: 1450–1458. <https://doi.org/10.1016/j.bpj.2011.08.003> PMID: 21943426
76. Tan C, Terakawa T, Takada S. Dynamic Coupling among Protein Binding, Sliding, and DNA Bending Revealed by Molecular Dynamics. *J Am Chem Soc*. 2016; 138: 8512–8522. <https://doi.org/10.1021/jacs.6b03729> PMID: 27309278
77. Terakawa T, Takada S. RESPAC: Method to Determine Partial Charges in Coarse-Grained Protein Model and Its Application to DNA-Binding Proteins. *J Chem Theory Comput*. 2014; 10: 711–721. <https://doi.org/10.1021/ct4007162> PMID: 26580048
78. Vasudevan D, Chua EYD, Davey CA. Crystal Structures of Nucleosome Core Particles Containing the '601' Strong Positioning Sequence. *J Mol Biol*. 2010; 403: 1–10. <https://doi.org/10.1016/j.jmb.2010.08.039> PMID: 20800598
79. Kenzaki H, Koga N, Hori N, Kanada R, Li W, Okazaki K, et al. CafeMol: A Coarse-Grained Biomolecular Simulator for Simulating Proteins at Work. *J Chem Theory Comput*. 2011; 7: 1979–1989. <https://doi.org/10.1021/ct2001045> PMID: 26596457